Available online at www.sciencedirect.com

ScienceDirect

Geochimica et Cosmochimica Acta 144 (2014) 277–298

Geochimica et Cosmochimica Acta

www.elsevier.com/locate/gca

Terminal particle from Stardust track 130: Probable Al-rich chondrule fragment from comet Wild 2

D.J. Joswiak [a,*], D. Nakashima [b], D.E. Brownlee [a], G. Matrajt [a], T. Ushikubo [b], N.T. Kita [b], S. Messenger [c], M. Ito [d]

[a] *Department of Astronomy, University of Washington, Seattle, WA 98195, USA*

[b] *Laboratory for Early Solar System Evolution, Division of Earth and Planetary Materials Science, Graduate School of Science, Tohoku University, Aoba, Sendai, Miyagi 980-8578, Japan*

[c] *Robert M. Walker Laboratory for Space Science, Johnson Space Center, ARES, Mail Code KR, 2101 NASA Parkway, Houston, TX 77058, USA*

[d] *JAMSTEC, Kochi Institute for Core Sample Research, 200 Monobe-otsu, Nankoku, Kochi 783-8502, Japan*

Received 29 January 2014; accepted in revised form 17 August 2014; Available online 27 August 2014

Abstract

A 4 × 6 μm terminal particle from Stardust track 130, named Bidi, is composed of a refractory assemblage of Fo_{97} olivine, Al- and Ti-bearing clinopyroxene and anorthite feldspar (An_{97}). Mineralogically, Bidi resembles a number of components found in primitive chondritic meteorites including Al-rich chondrules, plagioclase-bearing type I ferromagnesian chondrules and amoeboid olivine aggregates (AOAs). Measured widths of augite/pigeonite lamellae in the clinopyroxene indicate fast cooling rates suggesting that Bidi is more likely to be a chondrule fragment than an AOA. Bulk element concentrations, including an Al_2O_3 content of 10.2 wt%, further suggests that Bidi is more akin to Al-rich rather than ferromagnesian chondrules. This is supported by high anorthite content of the plagioclase feldspar, overall bulk composition and petrogenetic analysis using a cosmochemical Al_2O_3–Ca_2SiO_4–Mg_2SiO_4 phase diagram. Measured minor element abundances of individual minerals in Bidi generally support an Al-rich chondrule origin but are not definitive between any of the object types. Oxygen isotope ratios obtained from olivine (+minor high-Ca pyroxene)fall between the TF and CCAM lines and overlap similar minerals from chondrules in primitive chondrites but are generally distinct from pristine AOA minerals. Oxygen isotope ratios are similar to some minerals from both Al-rich and type I ferromagnesian chondrules in unequilibrated carbonaceous, enstatite and ordinary chondrites. Although no single piece of evidence uniquely identifies Bidi as a particular object type, the preponderance of data, including mineral assemblage, bulk composition, mineral chemistry, inferred cooling rates and oxygen isotope ratios, suggest that Bidi is more closely matched to Al-rich chondrules than AOAs or plagioclase-bearing type I ferromagnesian chondrules and likely originated in a chondrule-forming region in the inner solar system.

1. INTRODUCTION

Thousands of grains were collected by the Stardust spacecraft during its encounter with comet 81P/Wild 2 in February 2004 and were subsequently delivered to Earth in January 2006. Numerous high-temperature materials were recovered from their host aerogel tracks including Ca, Al-rich inclusions (CAIs) (Zolensky et al., 2006; Simon et al., 2008; Schmitz et al., 2009; Matzel et al., 2010; Joswiak et al., 2013), ferromagnesian (FMG) chondrule fragments (Nakamura et al., 2008; Gainsforth et al., 2010; Bridges et al., 2012; Joswiak et al., 2012;

* Corresponding author.
E-mail address: joswiak@astro.washington.edu (D.J. Joswiak).

http://dx.doi.org/10.1016/j.gca.2014.08.017
0016-7037/

Nakashima et al., 2012; Ogliore et al., 2012), possible amoeboid olivine aggregate (AOA) fragments (Nakamura-Messenger et al., 2011; Nakashima et al., 2012) and anhydrous mineral and rock grains (Zolensky et al., 2006; Joswiak et al., 2012). Presolar grains (Messenger et al., 2009; Leitner et al., 2010), organic materials (Sandford et al., 2006; Matrajt et al., 2008) and exotic sub-100 nm Ti, V nitride inclusions (Simon et al., 2008) were also found. Because of the diversity of materials discovered in Wild 2, this has led to the view that materials accreted to comet Wild 2 may have been derived from wide regions throughout the nebula (Brownlee et al., 2012). Many of the Wild 2 materials and their comparable chondrite counterparts could have formed contemporaneously in common reservoirs.

We studied the 4×6 μm terminal particle (TP) from track 130 (nicknamed Bidi), which has not previously been examined, and found that it is largely composed of Mg-rich olivine, Al- and Ti-rich clinopyroxene and anorthitic plagioclase and is therefore mineralogically similar to both Al-rich chondrules and amoeboid olivine aggregates (AOAs) leading to the suggestion that Bidi may have a similar origin as these objects. The minerals found in Bidi are also observed in some type I plagioclase-bearing ferromagnesian chondrules, thus a question is raised as to whether Bidi could be a type I ferromagnesian chondrule fragment rather than an Al-rich chondrule or AOA. Al-rich chondrules are composed of high-temperature minerals, principally Mg-rich olivine, Al- and Ti-rich clinopyroxene, anorthitic plagioclase ± spinel ± low-Ca pyroxene ± glass, and have textures similar to common ferromagnesian chondrules indicating their probable origin as crystallized melt droplets in refractory-rich regions in the solar nebula (Russell et al., 2000). Their mineralogical and chemical properties indicate that they may have links to both ferromagnesian chondrules and CAIs (Krot and Keil, 2002; Krot et al., 2002a,b; MacPherson and Huss, 2005). AOAs are fine-grained aggregates that are composed of similar refractory minerals as Al-rich chondrules. These objects may have formed by condensation of vapor in the early nebula (Krot et al., 2004a; Komatsu et al., 2009 and references therein). Because of their ^{16}O-rich compositions and mineral textures suggestive of condensation, AOAs may have petrogenetic links to CAIs (Itoh et al., 2007). Bidi, with its relatively refractory mineral assemblage, appears to be mineralogically distinct from most previously reported Stardust materials. Its derivation from Wild 2 continues to add to the growing list of high-temperature refractory objects found in the comet that appear to be linked to chondritic meteorites.

In several Stardust tracks, large (~2 to 6 μm) mineral and rock fragments have been reported that may have links to either AOAs or Al-rich chondrules. For instance, single forsterite grains lodged along track walls and found as terminal particles which are ^{16}O-rich and high in MnO are chemically and isotopically similar to olivine in certain types of AOAs (Weisberg et al., 2007; Nakamura-Messenger et al., 2011; Nakashima et al., 2012). A $\sim 2.4 \times 6.5$ μm Wild 2 terminal particle from track 154 and composed of Al-diopside with minor amounts of low-Ca pyroxene, Mg-rich olivine and pigeonite was suggested to be related to Al-rich chondrules (Bridges et al., 2012). Although these Wild 2 fragments are not composed of entire assemblages observed in either AOAs or Al-rich chondrules, they do offer tantalizing evidence that high-temperature refractory objects found in chondrites, besides ferromagnesian chondrules and CAIs, could be present in Wild 2.

Here we present the mineralogy, mineral chemistry, petrology, bulk composition and oxygen isotope measurements of the terminal particle Bidi and compare and contrast these properties to Al-rich chondrules, plagioclase-bearing type I ferromagnesian chondrules and AOAs to determine which object type, if any, Bidi may be related to. Because Bidi has an angular morphology and is not spherical like most chondrules, we refer to it as a fragment though we cannot be certain that it was derived from a larger pre-existing grain. To investigate textural relationships within Bidi and obtain mineralogical compositions, we used standard transmission electron microscopy (TEM) techniques on microtome sections and secondary electron microscopy (SEM) on the potted butt. Following these examinations, we measured oxygen isotopes on a microtomed thin section with a NanoSIMS ion microprobe and the potted butt with a IMS-1280 ion microprobe.

2. SAMPLE PREPARATION AND ANALYTICAL TECHNIQUES

The ~2.5 mm-long aerogel keystone (Westphal et al., 2004) containing track 130 (C2061,3,130) was obtained from the curatorial facility at the Johnson Space Center. It was flattened at the University of Washington Cosmic Dust Lab between clean glass microscope slides and embedded in a ~100 μm-thick slab of acrylic resin. After optical examination, the end of the track containing the terminal particle was cut from the remaining portion of the track and glued to the top of an acrylic cylinder approximately 1 cm in height and 7 mm in diameter. After cutting increasingly smaller stairstep mesas around the TP with a top mesa size of ~100 μm/side, the TP was microtomed with a 45 degree diamond knife on a Leica Ultracut S ultramicrotome. The microtomed sections, each approximately 70 – 100 nm-thick, were placed onto 200-mesh Cu or Au TEM grids containing 10 nm-thick C thin-films. See Matrajt and Brownlee (2006) for details of the embedding process and sample preparation techniques.

2.1. Electron microscopy

The microtome sections were studied with a Tecnai 200 keV field-emission TEM equipped with a bright-field/dark-field CCD camera and secondary electron and high-angle annular dark-field (HAADF) STEM (scanning transmission electron microscope) detectors. High-resolution lattice-fringe images and selected-area electron diffraction (ED) patterns were used to measure atomic spacings in individual minerals. The measured d-spacings and their associated angles obtained from the diffraction patterns were compared to X-ray diffraction (XRD) data from the

JCPDS Mineral Powder Diffraction File Data Book (Bayliss et al., 1980) to confirm mineral atomic structures. Well-known mineral standards were used for calibration of the high-resolution TEM images and electron diffraction ring patterns from an evaporated Al-thin film were used for calibration of camera length for electron diffraction. Estimated errors are less than 5% for both the HRTEM images and the electron diffraction patterns. Angular measurements between reflections in the diffraction patterns have errors of less than 2 degrees.

Energy-dispersive X-ray (EDX) spectra were obtained from samples that were placed in a low-background beryllium sample holder with double-tilt capability. An EDAX Genesis analysis system and light element X-ray detector were used to obtain and quantify all EDX spectra. To reduce volatilization and minimize electron beam damage, broad beam techniques consisting of condensing the beam to a diameter no less than 50–100 nm in conventional TEM mode were employed during acquisition of EDX spectra. Olivines and pyroxenes were generally quite robust during analyses showing little to no effects from electron beam exposure, however extra care was required when analyzing anorthite which was susceptible to irradiation damage, therefore electron beam current density was reduced during EDX analysis of this phase. Fitting and background subtraction routines using EDAX Genesis algorithms were employed to measure peak integrals. EDX spectral quantification was done by the thin-film k-factor element-ratio technique (Cliff and Lorimer, 1975). Si-normalized k-factors for O, Mg, Ca and Fe were measured using a NIST SRM 2063a thin-film standard while mineral standards were employed for all other elements. Spectral energy calibration was done using a Cu and Al thin-film prepared at the University of Washington. Estimated relative errors are less than 5% for major elements and ~30% for minor elements.

To complement TEM studies, we observed the Bidi potted butt with backscatter electrons (BSE) at 10 keV on a JEOL JSM 7000F FESEM located in the Materials Science and Engineering department at the University of Washington. To minimize damage to the acrylic resin, which is susceptible to shrinkage under the electron beam, BSE images were collected at low electron doses. The minerals in the potted butt were qualitatively confirmed with an attached EDX detector.

2.2. Oxygen isotope analysis

We performed isotopic measurements on a 70 nm-thick microtome thin section and of the potted butt of Bidi using a NanoSIMS 50L ion microprobe and an IMS-1280 ion microprobe, respectively. The isotopic measurements of the potted butt yielded higher precision compared with the microtome thin section due to the larger amount of mass measured, however, some IMS-1280 measurements which were obtained from ~1 × 2 μm spots overlapped with acrylic embedding medium. Although the isotopic precision obtained from the microtome section was lower, these measurements were obtained with a high spatial resolution (~100 nm) with negligible overlap with accessory phases or acrylic.

NanoSIMS images of $^{16}O^-$, $^{17}O^-$ and $^{18}O^-$ were acquired simultaneously with electron multipliers by rastering a 1 pA 16 keV primary Cs^+ ion beam focused to 100 nm. Measurements were performed at a mass resolving power (MRP) of >10,000 (Cameca NanoSIMS definition). Mass resolving power of the NanoSIMS (M/ΔM) is based on a definition where ΔM is the width in which 80% of the line intensity occurs. Under these conditions the $^{16}OH^-$ peak is resolved from the ^{17}O peak at a level below ~1‰. Isotopic compositions were determined with custom-written image processing software by defining regions of interest in images that correspond to specific mineral phases identified in TEM mineral maps. This software was also used to apply corrections for electron multiplier deadtime, quasi-simultaneous arrival and instrumental mass fractionation. Nearby, ~10 μm grains of San Carlos olivine were measured as oxygen isotopic standards. The high spatial resolution of the NanoSIMS isotopic images enabled mineral-specific oxygen isotope ratios to be obtained without significant contributions from adjacent acrylic. The initial results from these measurements are reported in Joswiak et al. (2010).

Oxygen isotope ratios were measured from the Bidi potted butt with a CAMECA IMS-1280 ion microprobe at the University of Wisconsin (WiscSIMS laboratory; Kita et al., 2009; Valley and Kita, 2009). Prior to the analyses, the sample was prepared at the University of Washington by cutting the acrylic mesa containing the sample and carefully pushing it into indium which filled a central 1.4 mm hole in a 8 mm Al disk. The disk containing Bidi and a 8 mm epoxy disk containing a San Carlos olivine grain (~1 mm) were mounted in a 25 mm diameter aluminum sample holding disk with three 8 mm holes which was developed for high-precision SIMS stable isotope analyses of cometary particles (Nakashima et al., 2011). The 1 mm San Carlos olivine grain that was loaded in the three-hole disk was used as a running standard for the Bidi analyses. Standardization of unknown samples using the running standard mounted in a different hole may induce a small mass-dependent fractionation at the level of 0.5–0.7‰ in $\delta^{18}O$ (Nakashima et al., 2011), though it does not affect $\Delta^{17}O$ values.

The analytical conditions and measurement procedures were similar to those in Nakamura et al. (2008) and Nakashima et al. (2012). A focused Cs^+ primary beam was set to ~1 × 2 μm and intensity of ~3 pA. Secondary ions of $^{16}O^+$ and $^{18}O^+$ were detected using a Faraday cup (FC) and electron multiplier (EM) on the multiple collector trolleys, respectively, with mass resolution (M/ΔM) of 2200 (where ΔM is the width at 10% peak height. The EM at the ion optical axis and fixed position (mono collection detector) was used for detection of $^{17}O^-$ to mass resolution 5000.

Intensities of $^{16}O^-$ were ~1.6×10^6 cps. The contribution of the tailing of $^{16}O^1H^-$ interference to $^{17}O^-$ signal was corrected by the method described in Heck et al. (2010), though the contribution was negligibly small (⩽0.1‰).

Five spots were analyzed in Bidi (Fig. 1) bracketed by nine sets of analyses on the San Carlos olivine grain mounted in an alternate hole in the three-hole disk. External reproducibility of the San Carlos olivine grain was 1.6‰ for $\delta^{18}O$, 1.8‰ for $\delta^{17}O$, and 2.0‰ for $\Delta^{17}O$ (2 SD), which are assigned as analytical uncertainties of unknown samples (see Kita et al. (2009, 2010) and Nakashima et al. (2012) for detailed explanations). We analyzed two plagioclase (An_{60} and An_{95}) and diopside standards (Valley and Kita, 2009; Kita et al., 2010) in the same session for correction of instrumental bias of plagioclase and high-Ca pyroxene. Individual data were carefully examined after the inspection of SIMS pits using an SEM (Hitachi S3400) and FESEM (Zeiss LEO1530) at the University of Wisconsin. Two of five analysis spots (spots 4 and 5) overlapped acrylic significantly (~50% to 80% in volume) (Fig. 1). Because the TP was originally present in aerogel the oxygen isotopic analyses of spots containing acrylic also include a component from aerogel. Data from spot 3 were obtained entirely from the interior of the fragment (olivine + high-Ca pyroxene) while oxygen ions from spots 1 and 2 were obtained from the edges of Bidi with slight to very slight overlaps with acrylic. The instrumental bias correction for the mixed analyses was applied as a mixture of olivine and high-Ca pyroxene.

3. RESULTS

3.1. Track description

A profile of the 1.3 mm-long track containing the TP Bidi is shown in Fig. 2a. The monotonically decreasing width of the track between the entry hole and the TP indicates that it is a type A track based on the classification scheme of Hörz et al. (2006) and discussed by Burchell et al. (2008). Type A tracks are typically carrot-shaped, thin and contain competent terminal particles that did not disaggregate during collection. Bidi is a 4 × 6 μm solid particle with little to no adhering fines. Optical examination of the track showed that it was exceptionally free of particles except for 2 or 3 micron-sized fragments located below the entry hole (see arrow in Fig. 2a). These fragments were not examined because of their small sizes. The original Bidi projectile size was estimated at ~5 μm from the experimental calibration curve of 'greatest track width' to 'original particle diameter' from Burchell et al. (2008) for type A tracks (their Fig. 2c).

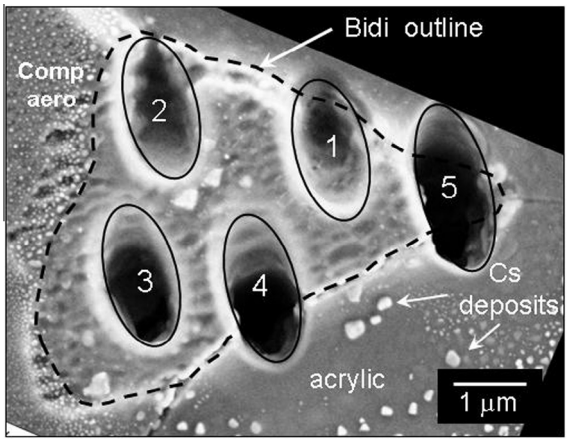

Fig. 1. SE image of potted butt showing pits after oxygen isotope analyses with CAMECA IMS-1280 ion microprobe. The perimeter of Bidi is shown by the dashed line. Material outside of this line is acrylic resin except for the upper left-hand side which is compressed aerogel attached to the fragment. Numbers refer to oxygen isotope analyses which are listed as 'Spot number' in Table 2. Due to overlaps with the surrounding acrylic, spots 1, 4 and 5 are not considered representative of the sample. Comp aero = compressed aerogel.

3.2. Bulk composition

Three largely intact microtome sections were used to estimate the bulk composition of Bidi. This was done by producing mineral maps of each microtome section from the TEM, summing pixels for each mineral phase over the three images (normalized to pixel size in each image) and combining these results with each average measured mineral composition. The calculated modal abundances are olivine 34%, clinopyroxene 33% and anorthite 33% showing that Bidi is composed of essentially equal amounts of these three phases.

Calculated mineral compositions (expressed in wt% oxide) of bulk Bidi are given in Table 1. Its bulk Al_2O_3 content of 10.2 wt% is at the lower end of the threshold of 10 wt% originally defined by Bischoff and Keil (1984) for Al-rich chondrules. Thus the measured bulk Al_2O_3 abundance of Bidi is within the realm of Al-rich chondrules.

3.3. Petrography, mineralogy and mineral chemistry

Bidi is a triangular-shaped grain 4 × 6 μm in size and is composed of MgO-rich olivine, clinopyroxene and anorthite-rich plagioclase (Figs. 2b and 3). In several microtome sections, olivine, pyroxene and anorthite appear to form a sequence with a layered or barred appearance (Fig. 3). This is also observed in the BSE image (Fig. 2b) which shows that clinopyroxene is sandwiched between olivine and anorthite. Moderate amounts of compressed to melted silica aerogel are often in sharp contact around the periphery of the particle. We did not observe any physical evidence of aerogel melt injected into interior portions of the fragment. From the TEM studies, well-defined anhedral to subhedral grain boundary contacts were observed between the major minerals. Like other Wild 2 samples that we have studied (Joswiak et al., 2012), we did not observe solar flare tracks in any Bidi phases.

In microtome sections, olivine was most often observed in direct contact with Ca-bearing pyroxene and only occasionally with anorthite. TEM diffraction patterns confirmed the olivine crystal structure. Bright- and dark-field TEM examination of the olivine revealed a uniform crystalline structure with few lattice defects or strain contrast. Measured Fe and Mg contents (Table 1) within the olivine showed little variation (Fa_{2-3}). Olivine MnO contents are low or below the detection limit of ~0.1 wt% (Fig. 4a).

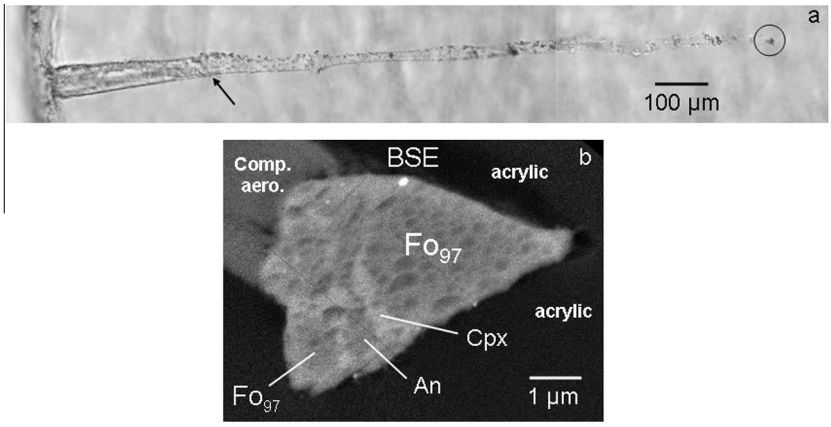

Fig. 2. (a) Transmitted-light image of 1.6 mm-long track 130 containing terminal particle Bidi (circle). The track is debris-free except for several micron-size fragments (arrow). Dark spots visible along the track are not fragments but are due to optical diffraction effects which disappeared after embedding in acrylic. (b) Field-emission SEM backscatter image of terminal particle Bidi in potted butt. The terminal particle is largely composed of three phases – Fo_{97}, clinopyroxene and anorthite. Clinopyroxene (Cpx) appears as brighter regions in the image and has a somewhat interstitial appearance. Bright rounded grains near the exterior of the TP are believed to be Fe metal. Large medium-gray "sail" on upper left is compressed aerogel which was produced during capture.

Table 1
Representative compositions of olivine, high-Ca pyroxene and anorthite/SiO_2 and bulk Bidi terminal particle (normalized oxide wt%).

Mineral	Olivine	High-Ca pyroxene	Anorthite (+SiO_2)	Bulk
SiO_2	42.93	55.62	57.97	52.02
TiO_2	b.d.	0.77	b.d.	0.37
Al_2O_3	0.20	6.53	25.39	10.2
Cr_2O_3	0.53	1.70	b.d.	0.72
FeO	1.88	1.11	0.08	1.34
MnO	0.17	b.d.	b.d.	0.03
MgO	54.07	16.45	0.81	25.59
CaO	0.23	17.82	15.45	9.61
Na_2O	b.d.	b.d.	0.30	0.09
Cations per 4 oxygen (olivine), 6 oxygen (pyroxene) and 8 oxygen (anorthite) anions				
Si	1.01	1.96	2.60	
Ti	b.d.	0.02	b.d	
Al	0.01	0.27	1.34	
Cr	0.01	0.05	b.d	
Fe	0.04	0.03	0.01	
Mn	b.d.	0.00	b.d.	
Mg	1.90	0.86	0.05	
Ca	0.01	0.67	0.74	
Na	b.d.	b.d.	0.03	
Fo, Wo/En, An	98	96/43	98	

Normative minerals shown for Bidi bulk composition in last column. b.d. = below detection.

When compared to AOAs and chondrules, Bidi olivine MnO abundances are most similar to Al-rich and plagioclase-bearing type I FMG chondrules (Sheng, 1992; Kita et al., 2000; Krot et al., 2004b; MacPherson and Huss, 2005; Kurahashi et al., 2008; Ushikubo et al., 2012; Wick and Jones, 2012) whose average olivine MnO contents are <0.1 wt%. In contrast, Cr_2O_3 abundances in Bidi olivine are relatively high with measured concentrations ranging up to 0.8 wt% (Fig. 4b). Because Cr easily diffuses out of olivine even at relatively mild metamorphic grades (Grossman and Brearley, 2005), the high Cr contents suggest that Bidi has not undergone significant heating. The Cr_2O_3 abundances measured in Bidi olivine overlap the highest Cr_2O_3 abundances in Al-rich chondrules, plagioclase-bearing type I FMG chondrules and AOAs from type 3.0–3.1 chondrites (Kita et al., 2000; Komatsu et al., 2001; Aléon et al., 2002; Krot and Keil, 2002; Krot et al., 2004b; MacPherson and Huss, 2005; Kurahashi et al., 2008; Ushikubo et al., 2012) (Fig. 4b).

Clinopyroxene exhibits distinct exsolution lamellae (Fig. 5a) with widths up to ~20 nm. Lattice-fringe widths of 0.95 nm (100) in the dark phase are in agreement with pigeonite while 0.46 nm (200) fringes in the bright phase

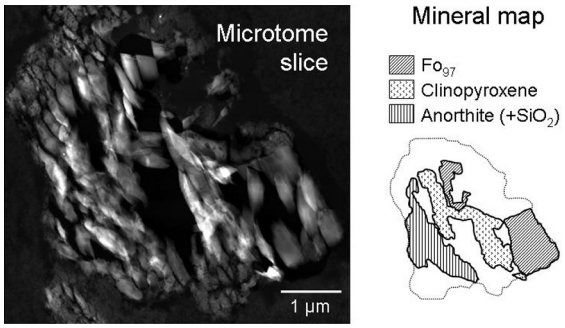

Fig. 3. High-angle annular dark-field (HAADF) image of microtome slice and corresponding mineral map from interior of terminal particle Bidi. Dark interior portions of HAADF image represent regions where shards were plucked out during microtoming. Aerogel melt is visible around exterior of much of the fragment and is outlined by dotted line on mineral map. Melt was not observed in interior portions of the particle. Minerals appear to define a upper-left to lower-right trending lineation.

match augite lattice planes, consistent with their primitive- and C-centered space groups, respectively. The complementary [0 1 0] electron diffraction pattern shown in Fig. 5b is composed of two overlapping diffraction patterns (augite and pigeonite) with coincidental c^* axes and non-overlapping a^* axes. Both augite and pigeonite crystallize in the monoclinic crystal system with similar but non-identical crystal lattices; this slight difference of several degrees in their β angles accounts for the non-coincidental a^* axes and the slight smearing in the reflections along the c^* direction in the diffraction pattern. Pigeonite and augite will exsolve from a parent clinopyroxene solid-solution during cooling at high-temperatures to accommodate strains within the crystal lattice. Undulating exsolution lamellae with terminations, which are exhibited in the Bidi pyroxenes, are characteristic of spinodal decomposition followed by grain coarsening during cooling (Weinbruch and Müller, 1995). Similar exsolution textures in diopside were reported in a ~4 μm terminal particle from SD track 69 indicating

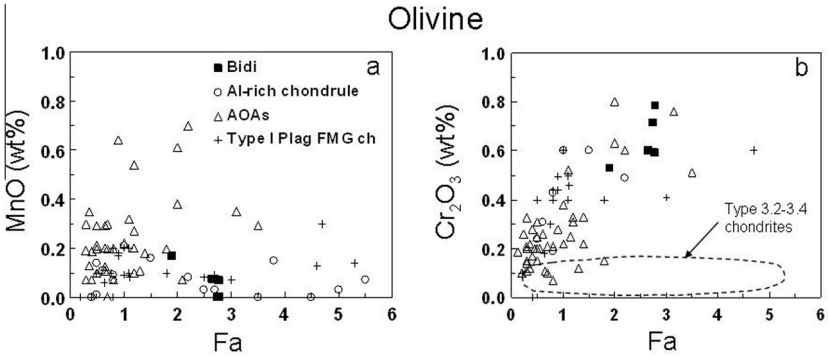

Fig. 4. Comparison of MnO (a) and Cr_2O_3 (b) abundances vs fayalite content in olivines from Bidi, Al-rich chondrules, plagioclase-bearing type I FMG chondrules and AOAs from unequilibrated ordinary and carbonaceous chondrites Acfer 094 and Adelaide. Region outlined by dotted line in (b) is from olivines in Al-rich and type I plagioclase-bearing FMG chondrules of petrographic type 3.2–3.4 in ordinary and carbonaceous chondrites. Legend in (a) applies to both figures. FMG = ferromagnesian, ch = chondrule. Data sources: Kita et al. (2000), Komatsu et al. (2001), Aléon et al. (2002), Krot and Keil (2002), Krot et al. (2004b), Weisberg et al. (2004), MacPherson and Huss (2005), Kurahashi et al. (2008), Ushikubo et al. (2012), Wick and Jones (2012).

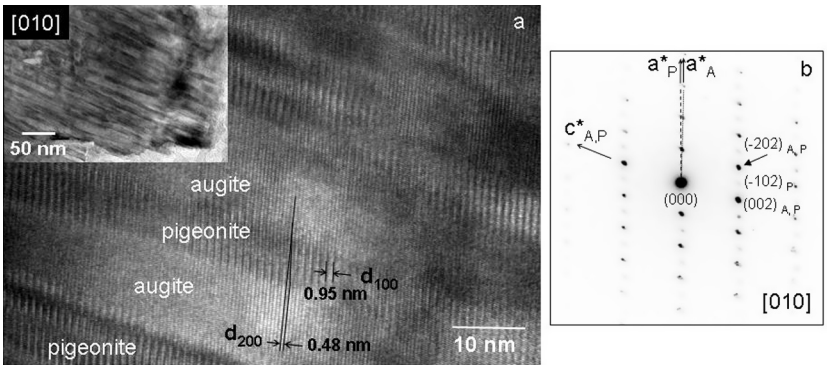

Fig. 5. (a) High-resolution image of intergrown augite and pigeonite lamellae looking down [0 1 0] zone axis. Well-defined, 0.95 nm-wide and 0.48 nm-wide (1 0 0) and (2 0 0) lattice fringes from pigeonite and augite, respectively, are shown. Inset shows diffraction contrast of undulating pyroxene structures in a wider field-of-view. (b) Corresponding [0 1 0] zone-axis diffraction patterns from augite and pigeonite. A small difference in the β angles results in a slight rotation between the diffraction patterns which appears as smearing in the reflections. A small direction change along (h 0 0) is also visible in the high resolution image (black lines). A = augite, P = pigeonite.

formation from a pre-capture high-temperature melt (Leroux et al., 2008).

Compositions obtained from Bidi pyroxenes are plotted in the pyroxene quadrilateral in Fig. 6. Bidi pyroxenes fall along a linear array on the Fe-poor side and spread from the diopside to the pigeonite fields. The large range in Ca contents (7.0–46.8 Wo%) is consistent with the exsolution textures of augite and pigeonite just discussed. The Ca contents of the Bidi pyroxenes have a similar range as the Ca contents in pyroxenes from Al-rich chondrules (Sheng, 1992; MacPherson and Huss, 2005) although Fe/Mg ratios are more variable in the latter. High-Ca pyroxene compositions from AOAs (solid ellipse, Fig. 6) and type I plagioclase-bearing FMG chondrules (dotted ellipse) have more restricted ranges in Ca content but have more similar Fe/Mg ratios when compared to Bidi pyroxenes (Komatsu et al., 2001; Aléon et al., 2002; Wick and Jones, 2012).

Variation diagrams of TiO_2, Cr_2O_3 and MnO vs. Al_2O_3 contents comparing Bidi clinopyroxene with clinopyroxenes in AOAs, Al-rich chondrules and type I plagioclase-bearing FMG chondrules from CR and type 3.0–3.1 OC and CC chondrites are shown in Fig. 7 (Brearley and Jones, 1998; Komatsu et al., 2001; Aléon et al., 2002; Krot and Keil, 2002; Krot et al., 2002a,b, 2004b; Weisberg et al., 2004; MacPherson and Huss, 2005; Kurahashi et al., 2008; Kita et al., 2010). Bidi pyroxenes contain moderate to relatively high abundances of TiO_2 (0.8–1.7 wt%) and Al_2O_3 (1.7–8.0 wt%) and are essentially indistinguishable from AOA and chondrule clinopyroxenes (Fig. 7a). The Cr_2O_3 contents of Bidi clinopyroxene are similar to clinopyroxenes in both Al-rich and plagioclase-bearing type I FMG chondrules but are clearly elevated from clinopyroxenes in AOAs (Fig. 7b). The MnO contents of high-Ca pyroxenes in many chondrules range from relatively high values of ~0.7 wt% to ~0.1–0.2 wt% which slightly overlap the highest measured MnO concentrations in Bidi clinopyroxene. Compared to the Al-rich and FMG chondrules, MnO abundances in AOA clinopyroxenes are generally low and much closer to MnO values in Bidi clinopyroxene. The high-Ca pyroxene element plots indicate that Al, Ti, Mn and Cr concentrations in Bidi are not entirely consistent with any one object type and therefore cannot be used to differentiate Bidi pyroxenes from pyroxenes from Al-rich chondrules, plagioclase-bearing type I FMG chondrules or AOAs.

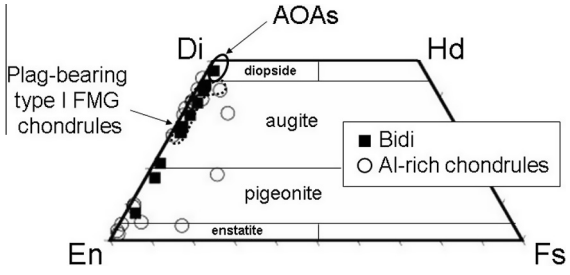

Fig. 6. Pyroxene quadrilateral comparing compositions of pyroxenes from Bidi, Al-rich chondrules, plagioclase-bearing type I FMG chondrules (dotted ellipse) and AOAs (solid ellipse). Bidi pyroxenes have low Fe abundances but span a large range in Ca contents similar to many Al-rich chondrules. Al-rich chondrule pyroxene compositions from Sheng (1992) and MacPherson and Huss (2005). Plagioclase-bearing Type I FMG chondrule field from Komatsu et al. (2001), Aléon et al. (2002) and Wick and Jones (2012). AOA pyroxene field from Aléon et al. (2002) and Komatsu et al. (2001).

The third major phase, anorthite, is found in regions up to 1.5 μm in size and is often in contact with pyroxene rather than olivine. TEM observations indicate that a pure SiO_2 phase is associated with the anorthite which is occasionally observed in alternating bands up to 100 nm-wide (Fig. 8a) and sometimes as well-defined lamellae. Measurements taken from the anorthite regions show that the SiO_2 abundance is variable. All EDX spectra obtained from these regions contain excess SiO_2 (Table 1) which we do not believe resulted from aerogel intrusion during capture (see Section 4). Electron diffraction patterns taken from the anorthite regions are consistent with anorthite (Fig. 8b, inset) XRD data (Bayliss et al., 1980). No additional diffraction spots are observed in the ED patterns indicating that the associated silica phase is amorphous. EDX measurements of the SiO_2 material indicate that it is pure or nearly pure silica glass. Though we were unable to obtain EDX spectra from pure anorthite without additional SiO_2, the excess silica in the spectra does not alter the Ca/(Na + Ca) ratios of the anorthite, therefore we can accurately report the anorthite contents of the Bidi feldspar. Values ranged from An_{94} to An_{100} with an average of An_{97}. MgO contents of the anorthite are surprisingly high with measured values up to 1.8 wt% (Fig. 9). These elevated MgO levels are comparable to the MgO contents reported from anorthites in AOAs (Komatsu et al., 2001; Weisberg et al., 2004; Krot et al., 2004b), Al-rich chondrules (MacPherson and Huss, 2005) and plagioclase-bearing type I FMG chondrules (Kurahashi et al., 2008; Ushikubo et al., 2012; Wick and Jones, 2012) from the lowest metamorphic grade chondrites (CR and type 3.0–3.1 OC and CC) (Fig. 9). MgO abundances in Al-rich and type I FMG chondrules from higher subtype chondrites are generally lower than most Bidi analyses (dashed and dotted fields, Fig. 9). Increasing thermal metamorphism drives MgO from plagioclase due to the increase in diffusivity of Mg in the feldspar structure with higher temperature (LaTourrette and Wasserburg, 1998). The high MgO content of Bidi anorthite suggests that Bidi is a pristine object that experienced little to no thermal metamorphism.

We observed infrequent rounded sub 50-nm Fe-rich inclusions in the anorthite believed to be Fe metal (Fig. 8b). EDX spectra collected from STEM spot analyses from the Fe beads show that the inclusions are typically Ni-free though small amounts of P, S and Cr may be present. A trace amount of Ni, however, was observed in at least one inclusion. Similar Fe-rich inclusions were also infrequently observed in the clinopyroxene. Fe–Ni inclusions were reported in anorthite in AOAs in CR chondrites (Weisberg et al., 2004) while unidentified submicron inclusions were reported in anorthite in Al-rich chondrules from the primitive C3.05 chondritic meteorite Yamato 81020 (Kurahashi et al., 2008).

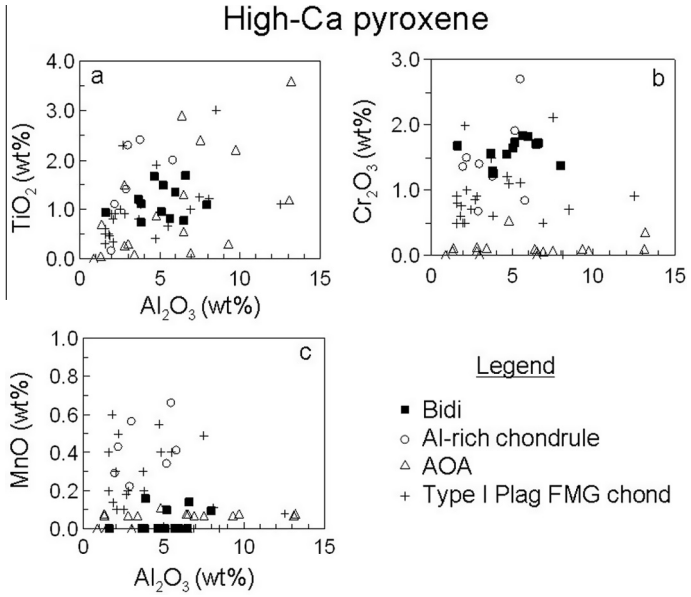

Fig. 7. TiO_2, Cr_2O_3 and MnO vs Al_2O_3 variation diagrams of high Ca-pyroxene in Bidi compared to Al-rich chondrules (Krot and Keil, 2002; MacPherson and Huss, 2005), AOAs (Komatsu et al., 2001; Aléon et al., 2002; Weisberg et al., 2004; Krot et al., 2004b) and plagioclase-bearing type I FMG chondrules (Brearley and Jones, 1998; Kurahashi et al., 2008; Kita et al., 2010) in CR and type 3.0–3.1 ordinary and carbonaceous chondrites. FMG = ferromagnesian.

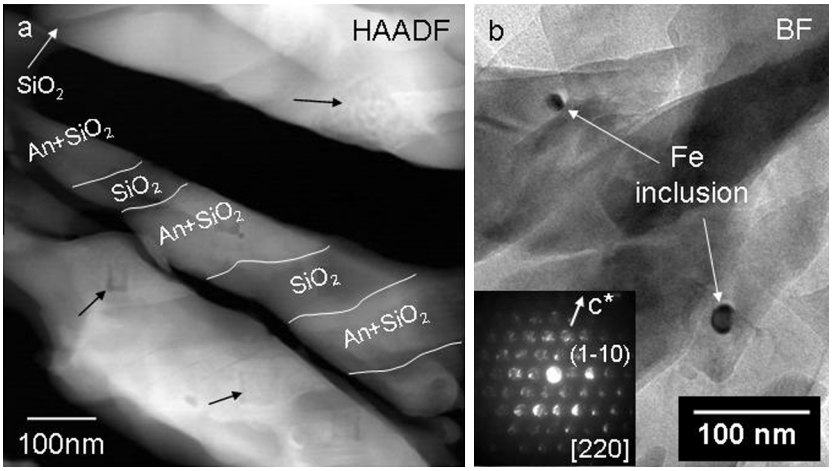

Fig. 8. (a) HAADF image of the interior portion of a microtome slice of Bidi showing alternating bands of anorthite/SiO_2 glass and SiO_2 glass. Poorly discernable circular features in upper-right and rectangular features on bottom-right and center-left of image are a result of irradiation damage by the electron beam (arrows). (b) Bright-field image of small portion of anorthite (+SiO_2 glass) with sub-50 nm round Fe inclusions. Diffraction pattern inset consistent with anorthite on [220] zone axis.

3.4. Oxygen isotopes

Oxygen isotope compositions obtained from the IMS-1280 on 5 Bidi spots (Fig. 1) are provided in Table 2 and plotted in the oxygen 3-isotope diagram in Fig. 10. The five analyses were obtained on different regions of the Bidi fragment believed to be largely olivine + minor pyroxene and incorporated different proportions of the embedding acrylic medium, except for spot 3 which was obtained entirely within the Bidi fragment (Table 2; Fig. 1). Beam overlaps with acrylic are significant because of potential high instrument mass fractionations (McKeegan et al., 2006; Nakashima et al., 2012). Oxygen from acrylic was present in the analyses from spots 1 and 4 and dominated the signal obtained from spot 5. This can be seen in Fig. 10 where spots 1 and 4 shift progressively towards lower $\delta^{17,18}O$ which lie on a mixing line between spot 5 in which the oxygen was primarily obtained from acrylic and spot 3, whose isotopic composition was obtained entirely from Bidi. The oxygen isotopic composition of spot 5 ($\delta^{18}O = -31.4‰$; $\delta^{17}O = -17.2‰$; $\Delta^{17}O = -0.9‰$) and the values obtained on acrylic from McKeegan et al.

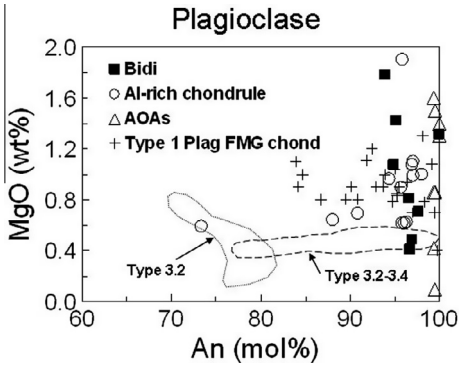

Fig. 9. Comparison of MgO vs anorthite contents in plagioclase feldspars from Bidi, Al-rich chondrules, AOAs and plagioclase-bearing type I FMG chondrules. High abundance of MgO in anorthite is an indicator of lack of thermal metamorphism of the feldspar. Al-rich chondrule anorthite data from Acfer 094 (ungrouped), Semarkona (LL3.00), Krymka (LL3.1), Acfer 182 (CH3) and CR chondrites EET 92042, EET 92147, PCA 91082, MAC 87320, and El Djour 001 (Krot and Keil, 2002; MacPherson and Huss, 2005; Ushikubo et al., 2012). AOA anorthite data from Adelaide, Acfer 094, Leoville (CV3.0) and CR chondrites EET 92-21, EET 87770, GRA 95229, MAC 87320 (Komatsu et al., 2001; Weisberg et al., 2004; Krot et al., 2004b). Anorthite data from plagioclase-bearing type I FMG chondrules from ALHA 77307 (CO3.0), Acfer 094 and Y-81020 (CO3.0) (Kurahashi et al., 2008; Ushikubo et al., 2012; Wick and Jones, 2012). Dashed elongate region shows anorthite contents from Al-rich chondrules from Chainpur (L3.4), Inman (L3.4), Quinyambie (L3.4) and Allende (CV3.2) (Sheng, 1992; MacPherson and Huss, 2005). Dotted region represents field of anorthite compositions from type I plagioclase-bearing FMG chondrules from Kainsaz (CO3.2) (Wick and Jones, 2012).

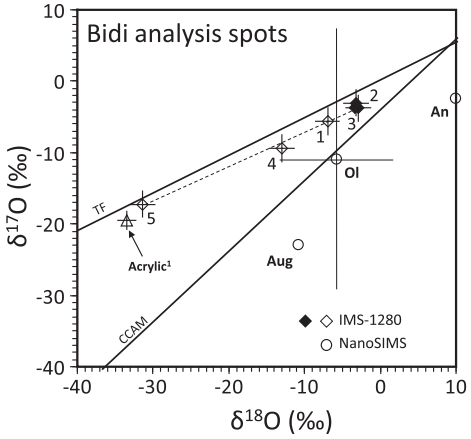

Fig. 10. Oxygen 3-isotope plot showing measured isotope compositions of 5 spots on Bidi potted butt from CAMECA IMS-1280 ion microprobe and 3 spots on a microtome slice with a NanoSIMS 50L ion microprobe. CAMECA IMS-1280 analyses are shown by open and solid diamond symbols that define array between TF and CCAM lines. These data define a mixing line between spot 3 obtained from analysis of pure Bidi and spot 5 largely obtained from embedding medium acrylic (see Fig. 1 and text for discussion). Spots 2 and 3 (solid diamond symbols) represent isotopic composition of pure or nearly-pure Bidi. Open circles show NanoSIMS analyses from olivine (Ol), augite (Aug) and anorthite (An). All error bars in the figure represent 2σ errors. Error bars not shown for NanoSIMS augite or anorthite which are greater than those shown for olivine. [1]Measured composition of acrylic (uncorrected) from McKeegan et al. (2006). TF = terrestrial fractionation line, CCAM = carbonaceous chondrite anhydrous mineral line.

(2006) ($\delta^{18}O = -33.5‰$; $\delta^{17}O = -19.5‰$) are similar. Bidi spots 2 and 3 provide representative oxygen isotope compositions from pure or nearly pure Bidi and therefore further oxygen isotopic discussions involving Bidi will be restricted to these two data points. Bidi points 2 and 3 plot between the TF and CCAM lines, although Bidi spot 2 slightly overlaps the TF line when 2σ errors are taken into account. Oxygen isotope measurements from the NanoSIMS are also shown in Fig. 10 and provided in Table 2. Although the oxygen isotopic images obtained from the NanoSIMS had sufficient spatial resolution (100 nm) to resolve the aerogel and discrete mineral phases, the small sample mass that was measured resulted in relatively low precision isotope measurements.

4. DISCUSSION

In chondrites, constituent components and their relationships to one another provide critical insights into their petrogeneses and origins. Isolated mineral clasts in matrix, for instance, which have similar compositions to comparable

Table 2
Oxygen isotope ratios (‰) obtained from Bidi fragment.

Spot #	Phase	Est. acrylic overlap	$\delta^{18}O \pm 2\sigma$	$\delta^{17}O \pm 2\sigma$	$\Delta^{17}O \pm 2\sigma$
			NanoSIMS		
	Fo_{97}	None	-5.7 ± 7.2	-10.9 ± 18	
	Augite	None	-10.8 ± 21.4	-23 ± 52	
	Anorthite	None	10 ± 50	-2.5 ± 74	
			IMS–1280		
1	Fo_{97}	Minor	-7.0 ± 1.6	-5.6 ± 1.8	-2.0 ± 2.0
2	Fo_{97} + aug	Trace	-3.2 ± 1.6	-3.1 ± 1.8	-1.4 ± 2.0
3	Fo_{97} + aug	None	-2.9 ± 1.6	-3.8 ± 1.8	-2.2 ± 2.0
4	Fo_{97}	Moderate	-13.0 ± 1.6	-9.4 ± 1.8	-2.6 ± 2.0
5	Fo_{97}	Significant	-31.4 ± 1.6	-17.2 ± 1.8	-0.9 ± 2.0

Est. = estimated, Fo = forsterite, aug = augite.

minerals in nearby chondrules might suggest genetic links between the clasts and chondrules and argue in favor of a process such as comminution, CAIs observed in the interior of chondrules would suggest younger chondrule ages compared to the CAIs (Misawa and Nakamura, 1996; Makide et al., 2009) or FeO-poor olivines found in type II chondrules would indicate material contributions from previous generations of chondrules (Jones, 1996). Bidi was an isolated terminal particle from a carrot-shaped track. Except for a few small submicron grains located near the entry hole, the track was clean and did not contain either capture-produced fine-grained materials or other large fragments, thus textural and compositional relationships to other possible associated materials could not be inferred. Comparison of Bidi's mineral assemblage, physical properties, major and minor element mineral abundances, bulk composition and oxygen isotope ratios to other chondrite components which are similar to Bidi may provide insight into its origin.

4.1. Chondrules and the size of Bidi

The size of the Bidi fragment, 4 × 6 um, is considerably smaller than conventional chondrules which have average diameters ~150 to 900 μm (with the exception of CH chondrites where average chondrule diameters are ~20 μm) (Rubin, 2010). A number of studies have found chondrules in the matrices and fine-grained rims of ordinary and carbonaceous chondrites with diameters of less than 40 μm (Rubin, 1989; Rubin et al., 1982; Wasson, 1993; Krot et al., 1997; Bigolski et al., 2013; Dobrică and Brearley, 2013). Dobrică and Brearley (2013) observed numerous spherical to subspherical microchondrules in matrix in the UOCs Semarkona (LL3.00) and MET 00526 (3.05) with average diameters of 6 μm. The microchondrules were variously composed of olivines, pyroxenes, Fe sulfides and glass and are believed to have formed in the same region as the larger chondrules. Krot et al. (1997) also reported frequent microchondrules in unequilibrated UOCs including Semarkona (LL3.00), Bishunpur (LL3.1), EET 90161 (L3.4), EET 90261 (L3.4) and Piancaldoli (L3.4). The microchondrules were observed in fine-grained matrix in the rims of FeO-poor porphyritic olivine chondrules. The authors suggested that the microchondrules may have formed from melting and reaccretion of surface materials from their host chondrules. In several CR chondrites Weisberg et al. (1993) found microchondrules and microfragments present in matrix and dark inclusions. Compositionally the microchondrules were similar to the larger chondrule types which were mainly type I ferromagnesian chondrules composed of Mg-rich olivines, pyroxenes, Fe, Ni metal and other phases. These studies extend the size range of chondrules to dimensions that are typically found in Wild 2. Thus, identification and classification of chondrules or chondrule-like materials from Wild 2 based on size constraints is not weakened by their small sizes. The origin of microchondrules and their relationship to other components in chondrites, however, is not well characterized and more studies are needed.

4.2. Evidence for pristine nature of Bidi

Measured minor element concentrations in Bidi minerals suggest that the fragment has not been subjected to significant thermal metamorphism. High Cr_2O_3 abundances measured in olivine (0.5–0.8 wt% Cr_2O_3) are similar to high Cr_2O_3 concentrations in olivines in unequilibrated ordinary and carbonaceous chondrites (sub-types 3.0–3.1) (see Figs. 4 and 5, Grossman and Brearley, 2005). LaTourrette and Wasserburg (1998) showed that Mg in feldspar diffuses into co-existing ferromagnesian silicates with increasing thermal metamorphism. In Bidi, high MgO values in the anorthite (average, 1.0 wt% MgO) are consistent with little to no heating. In Yamato-81020, a very primitive CO3.05 chondrite, Kurahashi et al. (2008) measured up to 1.1 wt% MgO in feldspar in type I chondrules and up to ~0.3 wt% MgO in plagioclase in Al-rich chondrules. In contrast, lower MgO contents present in the Kainsaz (CO3.2) plagioclase-bearing ferromagnesian chondrules were attributed to loss from mild metamorphism experienced by this chondrite (Fig. 9; Wick and Jones, 2012). Thus, the elevated concentrations of Cr in forsterite and Mg in anorthite provide direct evidence that Bidi experienced little to no thermal metamorphism indicating that it is likely to be a pristine object.

4.3. Bidi compared to Al-rich chondrules, plagioclase-bearing type I ferromagnesian chondrules and AOAs: mineralogical and chemical characteristics

A number of previous studies have shown that many Wild 2 particles have properties similar to objects observed in chondritic meteorites including ferromagnesian chondrules (Nakamura et al., 2008; Joswiak et al., 2012) and CAIs (Zolensky et al., 2006; Simon et al., 2008; Matzel et al., 2010; Ishi et al., 2010; Joswiak et al., 2013) while some particles from Wild 2 contain materials more characteristic of IDPs (i.e., Kool grains (Joswiak et al., 2009) and an enstatite whisker (Stodolna et al., 2012)). An important question is whether Bidi may have links to other known extraterrestrial objects or whether it formed in a region independent of these materials. Here we compare the mineral and chemical properties of Bidi to Al-rich chondrules, plagioclase-bearing type I FMG chondrules and AOAs, the objects which Bidi most resembles.

Al-rich chondrules are composed of mixtures of olivine, Al, Ti-rich clinopyroxene, Ca-rich plagioclase feldspar ± spinel ± low-Ca pyroxene ± glass, are texturally similar to some ferromagnesian chondrules and likely formed by crystallization of liquid droplets in the solar nebula (MacPherson and Huss, 2005; Tronche et al., 2007). Although less common than ferromagnesian chondrules, Al-rich chondrules are observed in all chondrite groups but are highest in abundance in carbonaceous chondrites (Franchi, 2008). A number of authors have suggested that Al-rich and ferromagnesian chondrules may be related groups of objects. For instance, anorthite-rich chondrules in CH and CR carbonaceous chondrites may have formed by melting of type I chondrule nebular precursors which mixed with refractory materials (Krot and Keil, 2002). In

ordinary chondrites, Al-rich and type I ferromagnesian chondrules define a continuous trend in oxygen isotopic compositions suggesting a close genetic relationship (Russell et al., 2000). MacPherson and Huss (2005) and Nagahara et al. (2008) showed that Al-rich chondrules may be linked to CAIs and ferromagnesian chondrules in a complex way involving volatility-controlled processes from gas–solid reactions of their precursors.

Amoeboid olivine aggregates (AOAs) differ from Al-rich and ferromagnesian chondrules by their finer-grained minerals and a general lack of glass. Pristine AOAs have ^{16}O-rich compositions and textures consistent with a condensation origin (Aléon et al., 2002; Krot et al., 2002a,b, 2004b; Weisberg et al., 2004; Itoh et al., 2007). In addition to olivine, clinopyroxene, anorthite and spinel, AOAs may also contain minor quantities of Fe, Ni-metal, perovskite or melilite (Krot et al., 2004b; Komatsu et al., 2009). Many AOAs contain secondary phases indicative of later reaction with solar nebula gas (Komatsu et al., 2009). Secondary minerals include anorthite, fayalitic olivine, Fe-rich pyroxenes and others and generally are significantly more ^{16}O-poor than their pristine counterparts. AOAs are observed in all the carbonaceous chondrite groups but rarely in ordinary chondrites and are apparently absent in enstatite chondrites (Scott and Krot, 2005a). Unlike Al-rich and ferromagnesian chondrules, mineralogical and isotopic differences between AOAs from different chondrite groups are not observed (Scott and Krot, 2005a).

Plagioclase-bearing type I FMG chondrules are observed in primitive chondrites including the CO3 and CR groups and Acfer 094 (Kurahashi et al., 2008; Tenner et al., 2012; Ushikubo et al., 2012; Wick and Jones, 2012). In general, type I chondrules contain olivine and low-Ca pyroxene minerals with Mg# $>$ 90 whereas olivines and pyroxenes in type II chondrules have Mg# $<$ 90. Plagioclase-bearing type I chondrules are composed of Mg-rich olivine, low-Ca pyroxene, Fe, Ni-metal, plagioclase feldspar and usually glass which is believed to be a primary phase. Many also contain high-Ca pyroxenes which are often observed as rims on Ca-poor pyroxenes or in mesostasis (Kurahashi et al., 2008). It is unlikely that Bidi is related to type II ferromagnesian chondrules because olivines and pyroxenes in these materials are much richer in Fe than equivalent phases in Bidi.

4.4. Minor elements

4.4.1. Olivine and high-Ca pyroxene

Minor element variations in Bidi olivine and pyroxene compared to Al-rich chondrules, plagioclase-bearing type I FMG chondrules and AOAs (Figs. 4 and 7) do not appear to unambiguously link Bidi with any of these object types (Type 3.0–3.1 chondrites). Although Cr_2O_3 abundances in Bidi olivine are more closely matched with AOA olivines (Fig. 4b) than Al-rich or plagioclase-bearing type I FMG chondrules, MnO abundances of Bidi olivine (Fig. 4a) do not uniquely match either AOAs or chondrules. In high-Ca pyroxenes, TiO_2 concentrations are indistinguishable between Bidi and the other object types (Fig. 7a), but Cr_2O_3 abundances are clearly elevated compared to AOAs (Fig. 7b) and are more similar to both Al-rich and type I plagioclase-bearing FMG chondrules. MnO abundances observed in Bidi high-Ca pyroxenes are most consistent with AOA high-Ca pyroxenes than either chondrule type, a result which is opposite to the Cr_2O_3 contents. Thus, minor element concentrations in the ferromagnesian minerals in Bidi are not exclusively consistent with a single object type, i.e., Al-rich chondrules, plagioclase-bearing type I FMG chondrules or AOAs.

4.4.2. Anorthite

Bidi anorthite is characteristically mixed at a fine-scale with silica glass occurring as well-defined layers, narrow lamellae and in irregular regions. Kitamura et al. (1977) showed that glass interlayered with anorthite could be produced by shocks, however, pressures of 15 GPa were required, a value much higher than the $<$1 GPa peak pressures that small ($<$10 μm) Wild 2 grains experienced during capture in aerogel (Anderson, 1998). Thus, shock pressures during capture are not likely responsible for the origin of the interlayered silica glass. Because of the regular alternating bands with anorthite it is unlikely to be incorporation or injection of silica aerogel during capture. Pristine AOAs do not contain amorphous silicates, however, silica is observed in Al-rich chondrules in Acfer 094 and CR and CH chondrites occurring in crystalline mesostasis with anorthite and high-Ca pyroxene (Krot and Keil, 2002; Krot et al., 2004a) as well as ferromagnesian cryptocrystalline chondrules in CH chondrites (Krot et al., 2000; Hezel et al., 2003; Nakashima et al., 2011). The Fe inclusions in Bidi anorthite could be the result of a reduction process. Small amounts of Fe are commonly present in the crystal lattices of plagioclase feldspars from chondrules in type 3 chondrites (Brearley and Jones, 1998). Iron contents in Bidi anorthite are low (0.0–0.51 wt%, average = 0.15 wt%) compared to Fe abundances in Al-rich chondrules which contain up to 0.9 wt% (average = 0.4 wt%) (Sheng, 1992; Krot and Keil, 2002; MacPherson and Huss, 2005). Thus, Fe in solid solution in the anorthite could have been the source of Fe that formed the inclusions in Bidi.

Bidi shares many mineralogical and chemical characteristics with AOAs, Al-rich chondrules and plagioclase-bearing type I FMG chondrules. Several important differences are evident, however. The first is the lack of low-Ca pyroxene and significant glass or mesostasis in Bidi which are characteristic phases in most type I chondrules. Some Al-rich chondrules and AOAs also contain low-Ca pyroxenes, but this phase is not common as in the ferromagnesian chondrules. Secondly, the MgO range and anorthite content of Bidi feldspar are more closely matched to Al-rich chondrules than either AOAs or the type I chondrules (Fig. 9). In AOAs, typical anorthite contents are higher than in Bidi, however, both have a similar range in MgO abundance. Anorthite contents measured in Bidi overlap a portion of measurements from anorthites in plagioclase-bearing type I chondrules which vary down to An_{84} (Kurahashi et al., 2008; Ushikubo et al., 2012; Wick and Jones, 2012), however the MgO contents are enriched in some Bidi anorthites compared to the type I chondrules (Fig. 9). Although these observations cannot be considered

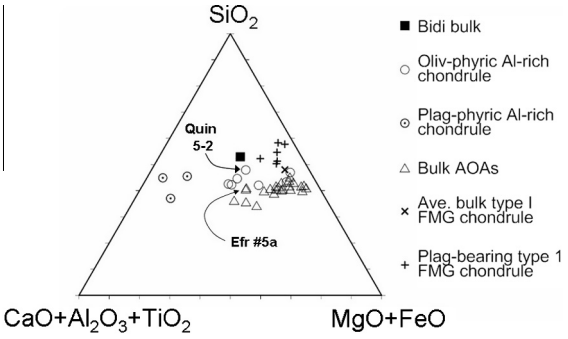

Fig. 11. $SiO_2 - MgO + FeO - CaO + Al_2O_3 + TiO_2$ ternary diagram (oxide wt%) showing bulk compositions of Bidi TP, Al-rich chondrules (oliv-phyric and plag-phyric), plagioclase-bearing type I FMG chondrules and AOAs. Also shown is the mean bulk composition of 11 type I FMG chondrules from Semarkona (Jones and Scott, 1989). Bulk compositions of Al-rich chondrule Quinyambie 6076-5-2 (MacPherson and Huss, 2005) and AOA Efremovka #5a (Komatsu et al., 2001) which plot closest to bulk Bidi are labeled in the figure.

strong evidence, they do suggest that Bidi may be more akin to Al-rich chondrules than either AOAs or plagioclase-bearing type I FMG chondrules.

4.5. Bulk composition

The bulk compositions of Bidi, Al-rich chondrules (Sheng, 1992; MacPherson and Huss, 2005), plagioclase-bearing type I FMG chondrules (Wick and Jones, 2012) and AOAs (Komatsu et al., 2001) are plotted in the $SiO_2 - MgO + FeO - CaO + Al_2O_3 + TiO_2$ ternary diagram in Fig. 11. Two subtypes of Al-rich chondrules are shown as olivine-phyric (oliv-phyric) or plagioclase-phyric (plag-phyric) based on the groups proposed by MacPherson and Huss (2005). Oliv-phyric and plag-phyric designate whether olivine or plagioclase, respectively, was an early crystallizing phase. Of these two groups, Bidi plots closer to Al-rich olivine-phyric chondrules suggesting that if Bidi formed as a liquid melt droplet in the nebula, then olivine likely crystallized before anorthite or clinopyroxene. When compared to AOAs, bulk Bidi is slightly richer in SiO_2. Average ferromagnesian chondrules, with or without plagioclase, plot close to the $SiO_2 - MgO + FeO$ side of the ternary diagram because of their lower concentrations of refractory elements compared to AOAs and Al-rich chondrules.

In CI-normalized El/Mg plots (Fig. 12, Palme and Jones, 2004), we compare bulk Bidi with oliv-phyric Al-rich chondrules (MacPherson and Huss, 2005) (Fig. 12a), plagioclase-bearing type I FMG chondrules (Wick and Jones, 2012) (Fig. 12b) and AOAs (Komatsu et al., 2001) (Fig. 12c). The normalized element concentrations and element patterns of many of the Al-rich chondrules and AOAs are more similar to Bidi than plagioclase-bearing type I FMG chondrules which generally have lower Al, Ca, Ti and Cr.

The Al-rich chondrules Chainpur 14-1 and Chainpur 20-1, described by MacPherson and Huss (2005) and Russell et al. (1996) are composed of Mg-rich olivine (Fo_{96-99}), anorthitic plagioclase and aluminous, Ti-bearing diopside, an assemblage nearly identical to Bidi. Minor euhedral spinels are present in the chondrules and are inferred as early liquidus phases in the crystallization of the aluminous chondrule melts. Spinel, however, was not observed in Bidi. The lower Al_2O_3 contents of Bidi (10.2 wt%) compared to Chainpur 14-1 ($Al_2O_3 = 16.2$ wt%), may account for the lack of this phase in the Wild 2 particle. We note that the Al-rich chondrule Quinyambie 6076-5-2, also discussed by MacPherson and Huss (2005) and Russell et al. (1996), is composed of olivine, sub-calcic augite and plagioclase (partly converted to maskelynite), has a similar bulk Al_2O_3 content (12.3 wt% vs 10.2 wt%) as Bidi and lacks spinel. In contrast, the bulk Al_2O_3 content (10.6 wt%) of the Chainpur 20-1 chondrule (Russell et al., 2000) does contain spinel grains (euhedral) although they are relatively rare. Regarding AOAs, the bulk composition of the AOA from the reduced CV chondrite Efremovka #5a has a remarkably similar El/Mg/CI pattern and bulk Al_2O_3 content (12.2 wt%) as Bidi but contains somewhat lower SiO_2 (Figs. 11 and 12c). The AOA is one of a large number of AOAs that are composed of fine-grained forsteritic olivine, aluminous diopside, anorthite and minor spinel. Like Al-rich chondrules, the mineral assemblages and major element contents of many AOAs are similar to Bidi.

Plots of the refractory oxides CaO vs Al_2O_3 and TiO_2 vs Al_2O_3 for bulk Bidi and bulk Al-rich chondrules, plagioclase-bearing type I FMG chondrules and pristine AOAs are shown in Fig. 13. The figures show that all object types plot along CI trends (Palme and Jones, 2004) including Bidi. The ferromagnesian chondrules define a much narrower range along the CI trend-line than AOAs and Al-rich chondrules. Bulk Bidi falls in the middle portions of the Al-rich chondrules and AOAs, but has higher CaO/Al_2O_3 and TiO_2/Al_2O_3 ratios than the ferromagnesian chondrules thus these oxide ratios in Bidi are more closely matched to Al-rich chondrules and AOAs than plagioclase-bearing type I FMG chondrules.

4.6. Cooling rates

Chondrules are believed to have crystallized very quickly from molten droplets in the nebula. From dynamic crystallization experiments and modeling of Fe–Mg zoning profiles in chondrule olivines, estimated cooling rates vary from ~10 to 1000 °C/h (Lofgren, 1996; Miyamoto et al., 2009). In principle, cooling rates can be estimated from the widths (wavelengths) of augite/pigeonite exsolution lamellae on (0 0 1) planes (Weinbruch and Müller, 1995). From the time–temperature–transformation (TTT) diagram provided by these authors (their Fig. 4) and our measured pyroxene wavelengths of 15–18 nm (Fig. 5), we estimate a cooling rate in the range of 100–1000 °C/h for Bidi pyroxene. This assumes an initial temperature of 1350 °C; cooling rates are greater for higher initial temperatures. If this estimated cooling rate is realistic, then Bidi may have formed in a chondrule-forming region where cooling rates up to >1000 °C/h occurred (Hewins, 1996) rather than a CAI-forming region where cooling rates were much lower, approximately a few tens of degrees/h (Stolper and Paque, 1986). Since AOAs are believed to have formed

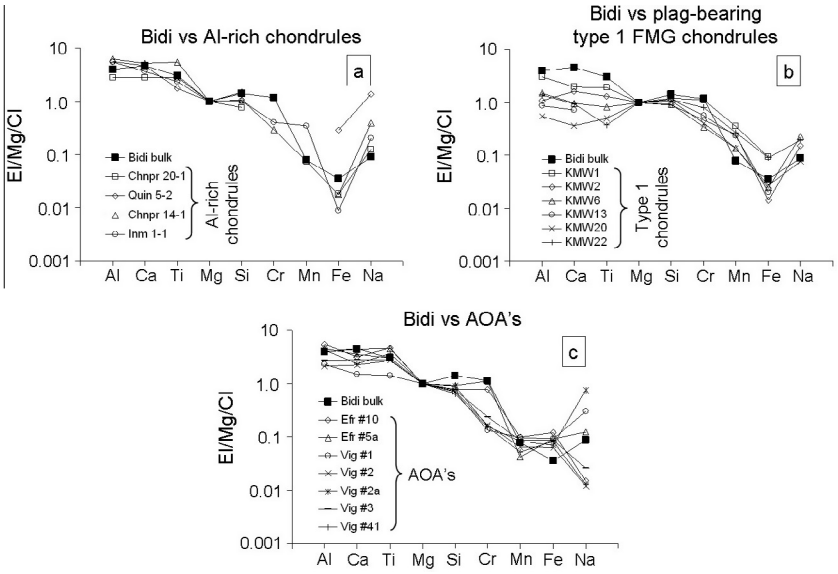

Fig. 12. El/Mg/CI-normalized plots of major and minor elements from bulk Bidi compared to bulk (a) oliv-phyric Al-rich chondrules (MacPherson and Huss, 2005), (b) plagioclase-bearing type I FMG chondrules (Wick and Jones, 2012) and (c) AOAs (Komatsu et al., 2001). Normalization values from Palme and Jones, 2004.

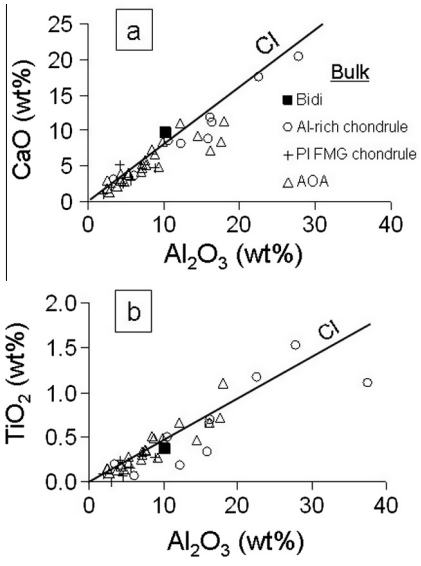

Fig. 13. CaO vs Al_2O_3 and TiO_2 vs Al_2O_3 in bulk Bidi, Al-rich chondrules (MacPherson and Huss, 2005), plagioclase-bearing type I FMG chondrules (Wick and Jones, 2012) and AOAs (Komatsu et al., 2001). CI-chondrite line calculated from values given by Palme and Jones (2004). Legend in upper plot applies to both figures.

in the CAI-producing regions (Scott and Krot, 2005a), our measured pyroxene cooling rates would favor Bidi as a chondrule (fragment) rather than an AOA.

4.7. Oxygen isotopes: Bidi compared to Al-rich chondrules and type I FMG chondrules

The oxygen isotope compositions of Bidi compared with Al-rich and plagioclase-bearing type I FMG chondrules from primitive carbonaceous, enstatite and ordinary chondrites are shown in Fig. 14. Our goal is to ascertain whether Bidi and comparable objects from the various chondrite types may have similar oxygen isotope ratios and thus possible genetic links. Because oxygen isotope data were not obtained from the bulk Bidi fragment but rather from small spots from the interior of the grain, principally olivine mixed with minor augite, we compare Bidi with oxygen isotope data from individual minerals from the chondrules rather than bulk analyses with a focus on olivine and high-Ca pyroxenes.

In Fig. 14a–d the oxygen isotope composition of Bidi is compared with similar minerals from CV3 and CR carbonaceous chondrites. The oxygen 3-isotope plots for Al-rich chondrules from CV3 (Allende and Mokoia) and CR chondrites (GRA95229, MAC87320, EET92042 and EET92147) (Fig. 14a and c) show that most olivines and high-Ca pyroxenes straddle the CCAM line in these groups (Maruyama and Yurimoto, 2003; Jones et al., 2004; Krot et al., 2006). The $\Delta^{17}O$ plots (Fig. 14b and d) indicate that olivines and pyroxenes from Al-rich chondrules from these chondrites have lower $\Delta^{17}O$ values than Bidi. Thus, isotopically Bidi does not appear to resemble Al-rich chondrules from primitive CV3 and CR chondrites.

How does Bidi compare with plagioclase-bearing type I FMG chondrules from these two groups? High-precision measurements of olivines from the plagioclase-bearing type 1 FMG chondrules from the CV3 chondrite Allende (Rudraswami et al., 2011) fall along a line slightly above the CCAM line but below the average of the two Bidi points. The trend of the CV3 FMG chondrule minerals marginally intersects Bidi spot 3 (Fig. 14a) when 2σ errors are taken into account. A few olivines have the same $\Delta^{17}O$ values (Fig. 14b) though most are lower or higher. Thus Bidi does have a similar oxygen isotope composition to

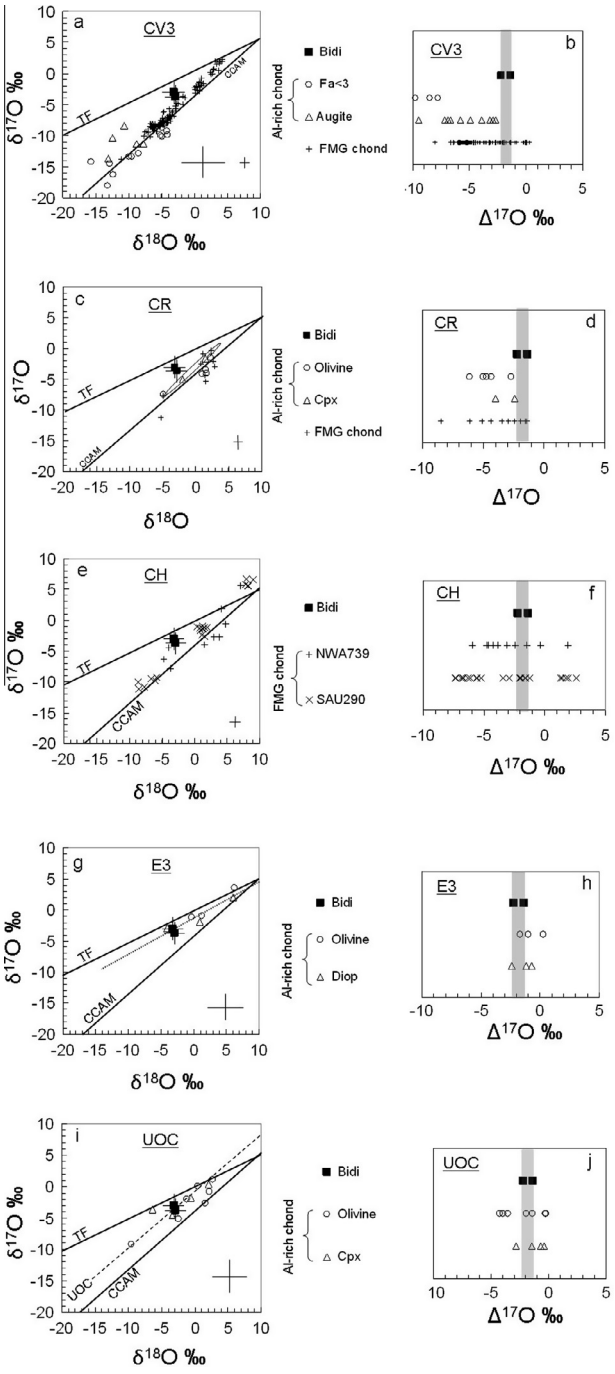

Fig. 14. Comparison of oxygen isotope compositions of Bidi to minerals (largely Mg-rich olivines and high-Ca pyroxenes) in Al-rich and type I plagioclase-bearing FMG chondrules from primitive chondrites in different chondrite groups and classes. In all plots Bidi is shown as solid squares, the Al-rich chondrules are shown by solid or open symbols and ferromagnesian chondrules are indicated by '+' or 'x' symbols. (a and b) Minerals from Al-rich chondrules from Allende (Maruyama and Yurimoto, 2003) and Mokoia (Jones et al., 2004) CV3 chondrites. Olivines from plagioclase-bearing type I FMG chondrules from Allende (Rudraswami et al., 2011). Large error bars in 3-isotope plot refer to average 1σ errors on Al-rich chondrule minerals. Small error bars (2σ) refer to higher precision measurements from ferromagnesian chondrule minerals. (c and d) Olivines and high-Ca pyroxenes from Al-rich chondrules from the CR2 chondrites GRA95229, MAC87320, EET92042 and EET92147 and olivines from plagioclase-bearing type I FMG chondrules from the same chondrites (Krot et al., 2006). Average 2σ error bars apply to both Al-rich and FMG chondrules. Elongate oval shows field of plagioclase-bearing type I FMG chondrules from the CR3 chondrite QUE99177 (Tenner et al., 2012). (e and f) Minerals from ferromagnesian chondrules from CH chondrites (Jones et al., 2005; Nakashima et al., 2011). One analysis from a pigeonite from NWA739 is hidden under one of the Bidi symbols. 2σ error bars in (e) refer to SAU290 chondrules from Nakashima et al. (2011). (d and h) Olivines and diopsides from Al-rich chondrules from EET 87746, LEW 87220 and Sahara 97072 E3 chondrites (Guan et al., 2006). 2σ error bars in (g) refer to Al-rich chondrules. (i and j) Olivines and high-Ca pyroxenes from Al-rich chondrules from unequilibrated ordinary chondrites (Russell et al., 2000). Dashed line labeled 'UOC' is the best-fit mixing line from Al-rich and ferromagnesian chondrules from unequilibrated ordinary chondrites (Russell et al., 2000). 2σ error bars in (i) refer to Al-rich chondrules. 2σ error bars shown for Bidi in all 3-isotope plots. Fa = fayalite, Cpx = clinopyroxene, Diop = diopside.

some plagioclase-bearing type I FMG chondrules from CV3 chondrites. A similar conclusion can be reached regarding plagioclase-bearing type I FMG chondrules from CR chondrites. High-precision oxygen isotope measurements from olivine + low-Ca pyroxene + plagioclase type I FMG chondrules from the CR3 chondrite QUE99177 (Tenner et al., 2012) fall above the CCAM line (oval in Fig. 14c) and along the Primitive Chondrule Mineral (PCM) line (not shown) (Ushikubo et al., 2012). Like the CV3 chondrites this line marginally intersects Bidi spot 3 within statistical error. Contrary to these results olivines and Ca-rich pyroxenes from plagioclase-bearing type I FMG chondrules from the CR chondrites EET92042 and MAC37320 from Krot et al. (2006) straddle the CCAM line and do not intersect Bidi. Although most $\Delta^{17}O$ values from the plagioclase-bearing type I FMG chondrules from Krot et al. (2006) have lower $\Delta^{17}O$ values, a few match Bidi. As shown by Nakashima et al. (2012), when Bidi Mg# is plotted against $\Delta^{17}O$, Bidi falls on the same trend as ferromagnesian minerals from chondrules from CR chondrites indicating that Bidi could have a genetic link to some CR chondrule minerals.

Chondrules from CH chondrites are intriguing analogous materials to chondrule-like fragments from Wild 2 because of their small sizes which can be as little as 20 μm (Scott and Krot, 2005a,b; Krot et al., 2006), a size approaching Bidi. Weisberg and Connolly (2008) proposed that some Wild 2 fragments have mineralogical and chemical similarities to CH chondrites suggesting possible affinities. Although type I chondrules from CH chondrites lack primary plagioclase we include a comparison to Bidi here because of possible links between Wild 2 chondrule-like grains and chondrules in CH chondrites. Oxygen isotope data from olivine and pyroxene minerals from selected type I ferromagnesian chondrules from the CH chondrites NWA739 (Jones et al., 2005) and from low-Ca pyroxenes (± minor olivines) from SaU290 (Nakashima et al., 2011) are shown in Fig. 14e and f. As of this writing, no oxygen isotope data from Al-rich chondrules from CH chondrites have been published. Olivines and pyroxenes from NWA739 and SaU290 display a relatively large range in $\delta^{17,18}O$ values; many fall on or around the CCAM line, on or above the TF line and occupy regions between the lines. Although several minerals from chondrules in NWA739 plot close to Bidi including single analyses from olivine ($Fa_{<10}$), low-Ca pyroxene and pigeonite (Jones et al., 2005) most have isotope compositions distinct from Bidi. The $\Delta^{17}O$ values of the FMG chondrule minerals span a relatively large range and most olivine and pyroxene minerals from type I FMG chondrules from CH chondrites are not isotopically similar to Bidi. However, a few do have comparable $\Delta^{17}O$ values, thus we cannot definitively rule out isotopic links between Bidi and chondrules from CH chondrites.

Recent high-precision oxygen isotope analyses of individual minerals from Al-rich and plagioclase-bearing type I FMG chondrules from the primitive chondrites Acfer 094 (ungrouped) and Y-81020 (CO3.05) have been reported (Ushikubo et al., 2012; Tenner et al., 2013). Although most of the $\Delta^{17}O$ values from olivines and pyroxenes are somewhat lower than Bidi, two plagioclase-bearing type I FMG chondrules from Acfer 094 have nearly identical $\Delta^{17}O$ values to Bidi indicating that Bidi and some chondrules from Acfer 094 may have links.

Both Al-rich and ferromagnesian chondrules are found in enstatite chondrites which formed under highly reducing conditions in the solar nebula (Guan et al., 2006; Krot et al., 2006; Weisberg et al., 2011). FeO-poor enstatite is the dominant phase in the ferromagnesian chondrules and is present in many Al-rich chondrules. Some Al-rich chondrules from enstatite chondrites contain olivine as well as diopside, plagioclase, spinel and glass (Guan et al., 2006). Oxygen isotope ratios of olivines and diopsides from six Al-rich chondrules from the unequilibrated enstatite chondrites EET87746, LEW87220 and Sahara 97072 (Guan et al., 2006) are shown in Fig. 14g and h. No plagioclase-bearing type I FMG chondrules have been reported from type 3 enstatite chondrites. The isotope ratios of most of the olivines and pyroxenes plot between the TF and CCAM lines and have similar $\Delta^{17}O$ values as Bidi within statistical errors. Minerals from the Al-rich chondrules define a regression line (unlabeled dotted line in Fig. 14g) with slope 0.6 ± 0.1 (Guan et al., 2006) which passes through the Bidi points. If there is significance to the regression line, then the concurrence of this line with Bidi and the similar $\Delta^{17}O$ values between olivines and pyroxenes suggests that Bidi could have originated in a source region that produced Al-rich chondrules in enstatite chondrites.

The oxygen isotope ratios of olivines and high-Ca pyroxenes from Al-rich chondrules from the unequilibrated ordinary chondrites Quinyambie (L3.4), Chainpur (LL3.4) and Sharps (H3.4) (Russell et al., 2000) along with Bidi are shown in Fig. 14i and j. In the 3-isotope diagram (Fig. 14i) the olivines and high-Ca pyroxenes from the Al-rich chondrules, like Bidi, largely fall between the TF and CCAM lines and some have similar $\delta^{17}O$ and $\delta^{18}O$ values. A best-fit 'UOC' line defined by olivine, clinopyroxene, plagioclase and spinel minerals from the UOC Al-rich chondrules (Russell et al., 2000) intersects the two Bidi data points. A number of olivines and high-Ca pyroxenes from the UOCs and Bidi also have similar $\Delta^{17}O$ values. Thus Bidi could have isotopic links to Al-rich chondrules from UOCs.

Comparison of the isotopic composition of Bidi olivine (+ augite) to olivine and Ca-rich pyroxene minerals in Al-rich chondrules and plagioclase-bearing type I FMG chondrules in carbonaceous, enstatite and ordinary chondrites of low petrologic subtypes shows that Bidi matches Al-rich and plagioclase-bearing type I FMG chondrules from a number of chondrite types. Because oxygen 3-isotope trend lines in Al-rich chondrules in UOC and E chondrites directly intersect Bidi and are located between the TF and CCAM lines, this might indicate that Bidi is more likely to be related to these objects than Al-rich chondrules from carbonaceous chondrites.

4.8. Could Bidi be an amoeboid olivine aggregate?

Amoeboid olivine aggregates are the most widespread types of refractory inclusions found in many types of

carbonaceous chondrites including CM, CR. CI, CV, CO, some ungrouped CCs (Krot et al., 2004b) and OCs (Itoh et al., 2007). In many primitive CCs, AOAs are mixtures of forsterite, Al-rich high-Ca pyroxene, anorthite, spinel ± Fe, Ni-metal ± low-Ca pyroxene ± melilite and display small to moderate effects of alteration, thermal metamorphism and melting (Krot et al., 2004b; Scott and Krot, 2005a). Many are fine-grained and some have porous textures suggestive of aggregation of solid grains. These and other properties have led to the supposition that AOAs may be objects that formed by accretion of solid refractory grains in the solar nebula which could be related to CAIs (Weisberg et al., 2004; Krot et al., 2004b). Often AOAs, like those in reduced CV chondrites, have textures composed of fine-grained mineral sequences of anorthite ± minor spinel, Al-diopside and olivine (Fagan et al. 2004), the mineral sequence observed in Bidi. Similarly, Bidi is composed of fine-grained minerals and does not have a spherical shape, properties more consistent with AOAs than chondrules.

We have shown that Bidi olivine contains a high concentration of Cr_2O_3 and that MgO levels in Bidi anorthite are similarly elevated, chemical properties that are inconsistent with thermal metamorphism. This indicates that Bidi is unlikely to be an AOA that was thermally altered even though Bidi does have similar oxygen isotope ratios to some altered AOAs (Imai and Yurimoto, 2003). Could Bidi then represent a pristine AOA? In a study of refractory high-Ca pyroxene, olivine and anorthite from AOAs in the Semarkona meteorite (LL3.00) Itoh et al. (2007) showed that these minerals were all enriched in ^{16}O ($\delta^{17,18}O = \sim -45‰$ to $-50‰$). Similarly, Aléon et al. (2002) measured ^{16}O-rich oxygen in individual minerals from four AOAs from CR chondrites whose $\delta^{17}O$ and $\delta^{18}O$ values ranged from $-39.2‰$ to $-48.4‰$ and $-34.5‰$ to $-50.3‰$, respectively. Other studies have obtained similar results (Hiyagon and Hashimoto, 1999; Krot et al., 2004b). However, the oxygen isotope composition of Bidi is relatively ^{16}O-poor and therefore Bidi is isotopically inconsistent with pristine AOAs. Additionally, the calculated fast cooling rates of 100–1000 °C/h calculated from the widths of exsolution lamellae in Bidi augite/pigeonite are more consistent with the rapid cooling of chondrules (see above) than AOAs. These, criteria suggest that Bidi is unlikely to be an AOA, either altered or pristine.

4.9. Comparison to Wild 2 chondrule fragments

Previous studies of fragments recovered from Stardust tracks indicate that some Wild 2 particles have mineral assemblages, textures and oxygen isotope compositions consistent with ferromagnesian chondrules (Nakamura et al., 2008; Nakashima et al., 2012; Ogliore et al., 2012). Several particles studied by Nakamura et al. (2008) have distinct igneous textures and are composed of mixtures of olivine, low-Ca pyroxene, Na, Ca-rich aluminosilicate glass, minor quantities of chromite and Fe, Ni-metal grains (T35/Torajiro, T108/Gozen-sama and Gen-chan). Isotopically, these Wild 2 chondrule fragments span a large range in $\delta^{17,18}O$ and none fall on or above the TF line leading the authors to conclude that the Wild 2 fragments are not related to ordinary, enstatite or R chondrites and therefore are most similar to ferromagnesian chondrules from carbonaceous chondrites. Nakashima et al. (2012) measured oxygen isotope compositions from nine Wild 2 particles including FeO-rich olivines and low-Ca pyroxenes, LIME forsterites and a FeO-rich olivine + diopside assemblage. Based on correlation trends between the $\Delta^{17}O$ and Mg# of these minerals and results from previous studies, Nakashima et al. (2012) suggested that many of the fragments were similar to chondrules from CR chondrites indicating possible formation of the Wild 2 particles from nebular environments where CR chondrites formed. In another study, a fragment named Iris from track 74, composed of a mixture of $Fa_{32–40}$ olivine, chromite, sodic plagioclase ($An_{14–22}$) and glassy mesostasis, resembles type II chondrules (Ogliore et al., 2012). Measurements taken from the olivine, chromite and mesostasis show that the fragment contains isotopically heavy oxygen as the Iris phases plot near the intersection of the CCAM and TF lines. Bridges et al. (2012) presented mineralogical and oxygen isotope data on a sub-terminal particle from Stardust track 154. The fragment consists largely of Al-rich diopside with minor amounts of olivine, low-Ca pyroxene and pigeonite. From oxygen isotope measurements obtained from the fragment by NanoSIMS and a TEM study of the minerals, the authors suggested the fragment had an origin consistent with Al-rich chondrules from carbonaceous chondrites. Two large fragments from track 26, named Ada, are composed of nodules of crystalline silica, believed to be tridymite, with rims of MnO-rich fayalite (Zolensky et al., 2006; Joswiak et al., 2012). The unique mineralogy of these fragments is strikingly similar to chondrules from some type 3 unequilibrated ordinary chondrites (Brigham et al., 1986; Wasson and Krot, 1994) suggesting that the particles from track 26 are also silica-rich chondrule fragments.

How does Bidi compare with these Wild 2 chondrule fragments? Mineralogically, Bidi is composed of Fo_{97} olivine, Al, Ti-rich clinopyroxene and An_{96} plagioclase and does not contain low-Ca pyroxene, spinel or mesostasis. Bidi does not have the same mineral assemblage as any other Wild 2 particle from any track and is therefore a mineralogically unique Wild 2 particle. Isotopically, however, Bidi appears to fall midway between the more isotopically heavy Wild 2 particles ($\delta^{18}O$ values range from $-12.2‰$ to $+9.0‰$ and $\delta^{17}O$ from $-10.8‰$ to $+5.9‰$), many of which plot between the TF and CCAM lines (Fig. 15). Measured $\Delta^{17}O$ values of Bidi olivine ($\Delta^{17}O = -1.4‰$ to $-2.2‰$) are essentially indistinguishable from a number of FeO-poor Wild 2 particles (Mg# > 90) which were shown by Nakashima et al. (2012) to have similar Mg# – $\Delta^{17}O$ trends as chondrules in CR chondrites. Although there is no a priori reason to expect that Bidi and the other Wild 2 grains are genetically linked, the isotope data support the idea that some of the Wild 2 grains could have a common source region. We note that, like chondrites, Wild 2 apparently contains a variety of chondrule types including ferromagnesian chondrules, Al-rich chondrules and

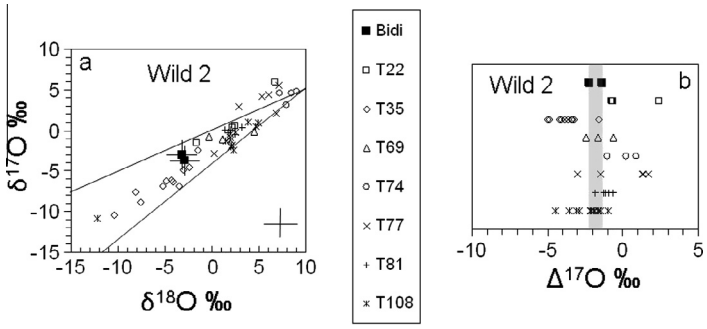

Fig. 15. Oxygen 3-isotope and $\Delta^{17}O$ plots showing Bidi compared to (mostly) olivines and low-Ca pyroxenes from Stardust tracks 22, 35, 69, 74, 77, 81 and 108 (Nakamura et al., 2008; Nakashima et al., 2012; Ogliore et al., 2012). Typical 2σ error bars shown in (a) except for track 81 which are approximately 40% larger in $\delta^{18}O$ but comparable in $\delta^{17}O$.

possible silica-bearing chondrules but it is unclear at present what relationship, if any, these chondrules have to one another.

4.10. Al-rich chondrules: Bidi petrogenesis

We showed that Bidi is more likely to be a chondrule fragment than an AOA because of its oxygen isotope composition and a higher inferred cooling rate (from pyroxene microstructures) that is more consistent with chondrules than AOAs. Also, bulk composition and minor element concentrations suggest that Bidi more closely matches Al-rich chondrules than the other object types. If Bidi is an Al-rich chondrule (or fragment) and formed similarly to Al-rich chondrules in chondrites, then it should have a predictable petrogenesis based on its bulk composition, mineral assemblage and mineral compositions. To look at this further we utilize the cosmochemical Al_2O_3–Ca_2SiO_4–Mg_2SiO_4 diagram provided by MacPherson and Huss (2005). The diagram is composed of primary liquidus fields defined by reaction boundaries and cotectic curves (Fig. 16). Strictly speaking, bulk compositions plotted on the diagram should be spinel saturated as the ternary diagram is a projection from spinel. The bulk composition of Bidi indicates that Bidi is not spinel saturated and would plot below local spinel saturation contours (not shown on the diagram). However, in crystallization experiments of Al-rich chondrule melts, Tronche et al. (2007) found that even with melts below spinel saturation valid mineral equilibria can be predicted with the phase diagram. Likewise, MacPherson and Huss (2005) show that the phase diagram predicts valid mineral assemblages for melts (Al-rich chondrules like Quinyambie 6076-5-2 that do not contain spinel) that are spinel undersaturated like Bidi. Therefore, with this caveat in mind we will use the diagram to discuss possible Bidi petrogenesis.

Bidi plots in the Fo liquidus field and near the center of the shaded region which shows the bulk compositions of Al-rich chondrules (MacPherson and Huss, 2005). Additionally, Bidi plots in the portion of the Al-rich chondrule field defined as Al-rich oliv-phyric chondrules (Fo + L field) and just to the left side of the thermal divide (join connecting An_{97} and Fo_{97}). AOAs also plot in the Fo liquidus field but generally at lower Al_2O_3 and do not overlap the

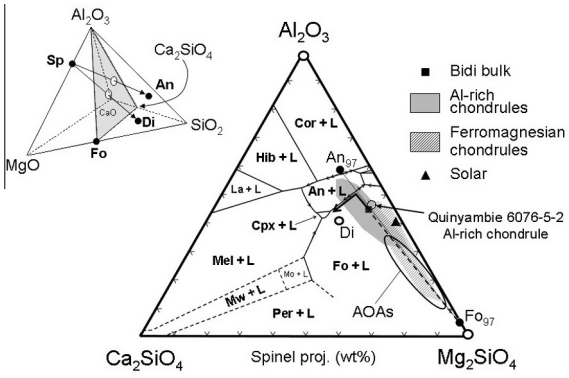

Fig. 16. Larnite-forsterite-corundum liquidus ternary diagram projected from spinel in CMAS tetrahedron. A melt with composition equivalent to bulk Bidi (black square) will crystallize olivine (and spinel) as the liquidus phase followed by anorthite and finally a high-Ca pyroxene (dark heavy arrowed line segment) due to its position in the Fo (+Sp) liquidus field and location to the left of the thermal divide (join between An_{97} and Fo_{97}). Al-rich chondrule and ferromagnesian chondrule fields from MacPherson and Huss (2005) and AOA field from Komatsu et al. (2009) and Krot et al., (2004a). All liquidus fields include spinel. The three small unmarked liquidus regions midway between Al_2O_3 and Mg_2SiO_4 are mullite + liquid, sapphirine + liquid and cordierite + liquid (top to bottom).

Bidi composition. Ferromagnesian chondrules plot in a region extending from the approximate location of Bidi toward the Mg_2SiO_4 apex and like Al-rich chondrules straddle the thermal divide. A melt composed of a bulk composition equal to Bidi (black square) will first crystallize forsteritic olivine, approximately Fo_{97} (determined using MELTS equilibria modeling (Ghiorso and Sack, 1995)). With falling temperature, the melt composition will reach the olivine–anorthite reaction boundary (dark black line segment in the figure), anorthite will begin to co-crystallize with olivine and the evolving melt composition will abruptly turn and follow the reaction curve (dark arrowed line segment) toward the clinopyroxene liquidus field. With continued falling temperature, the melt moves along the anorthite–olivine reaction boundary toward clinopyroxene because the original bulk composition is located on the Ca_2SiO_4-rich side of the An_{97}–Fo_{97} thermal divide. Along

this boundary, spinel (if present) can be consumed by reaction with the liquid thus accounting for spinel-free assemblages in some Al-rich chondrules (MacPherson and Huss, 2005) and perhaps Bidi. Finally Ca-rich pyroxene will crystallize as the melt reaches the clinopyroxene liquidus field. In Bidi, Ca-rich pyroxene is observed sandwiched between olivine and anorthite thus Bidi has a texture consistent with a predicted Al-rich chondrule crystallization sequence (Fig. 16). We point out that Quinyambie 6076-5-2, a spinel-undersaturated Al-rich chondrule, (MacPherson and Huss, 2005) which plots in the same location as Bidi is composed of nearly identical minerals and appears to have followed a similar crystallization path. Thus an inferred petrogenesis of Bidi is consistent with igneous crystallization similar to Al-rich chondrule melts.

4.11. Source regions

Previously we showed that the oxygen isotope composition of Bidi is similar to chondrules from a number of chondrite types including ordinary, enstatite and some carbonaceous chondrites. Because Bidi is composed of a mineral assemblage similar to Al-rich chondrules and has a bulk composition like many Al-rich chondrules, including $Al_2O_3 > 10$ wt%, it is likely that Bidi is also an Al-rich chondrule (fragment) rather than a plagioclase-bearing FMG chondrule. Because Bidi is an isolated grain from a track that was essentially free of additional debris it has no associations with other components unlike conventional meteorites whose provenances can be established, thus Bidi could have its origin from an ordinary, enstatite or carbonaceous chondrite region.

If Bidi is an Al-rich chondrule fragment, then it must have formed at temperatures $> \sim 1000$ °C similar to Al-rich chondrule analogs (Tronche et al., 2007) and may have formed in the chondrule-forming region of ~2 to 10 AU (Scott and Krot, 2005b) in the inner solar nebula. The high MgO content of the Bidi anorthite and the elevated Cr abundances in olivine indicate that Bidi did not reside in a large parent body prior to encapsulation in Wild 2, at least one that experienced significant thermal metamorphism, thus Bidi may have been accreted to comet Wild 2 directly from a chondrule-producing nebular environment without significant heating after its formation. As comets formed in the cold, outer reaches of the Solar System at distances of tens of AU from the Sun, Bidi must have been transported a vast distance to have been incorporated in a growing comet Wild 2. This could have been accomplished in a bipolar outflow as discussed in the Shu et al. (1997) X-wind model or perhaps via radial transport in a turbulent nebula (Bockelée-Morvan et al., 2002; Keller and Gail, 2004; Ciesla, 2007; Cuzzi et al., 2008).

5. CONCLUSIONS

The 4×6 μm terminal particle, Bidi, from Stardust track 130, an essentially debris-free, carrot-shaped track, is composed of MgO-rich olivine (Fo_{97}) and Al- and Ti-rich clinopyroxene and anorthite feldspar (An_{97}), major minerals that are observed in Al-rich chondrules, many amoeboid olivine aggregates and some type I FMG chondrules. Some major and minor element abundances in Bidi minerals are most consistent with corresponding minerals in Al-rich chondrules. The measured 10.2 wt% Al_2O_3 abundance of bulk Bidi also suggests that Bidi is more likely to be an Al-rich chondrule than a plagioclase-bearing type I FMG chondrule. Measurements of the widths of augite/pigeonite lamellae suggest that Bidi pyroxene experienced high cooling rates, a property more consistent with chondrules than AOAs. Petrogenetic analysis, using the measured bulk composition of Bidi and a cosmochemical phase diagram applicable to AOAs, Al-rich and FMG chondrules, is consistent with the crystallization of Bidi minerals similar to Al-rich chondrules.

Oxygen isotope ratios obtained from olivine (+ minor augite) show that Bidi falls midway between the TF and CCAM lines at intermediate $\delta^{17,18}O$ values and has $\Delta^{17}O$ values of $-1.4‰$ to $-2.2‰$. On an oxygen 3-isotope plot Bidi falls in a region overlapping MgO-rich olivines and high-Ca pyroxenes from Al-rich chondrules from several primitive chondrite types including unequilibrated ordinary, enstatite and some carbonaceous chondrites and has similar $\Delta^{17}O$ values to many of the minerals from these chondrites. Oxygen isotope ratios are not sufficient to uniquely determine if Bidi may be genetically related to any particular chondrite group or class but are closest to Al-rich chondrules from ordinary or enstatite chondrites. Bidi does not isotopically match minerals from pristine AOAs which are ^{16}O-rich, therefore, it is unlikely that Bidi has an origin as an AOA.

Taken together, the bulk composition, mineral assemblage, some major and minor elements in constituent minerals, calculated fast cooling rates and oxygen isotope ratios in Bidi are consistent with an Al-rich chondrule (fragment). Because of high MgO contents in anorthite as well as elevated Cr_2O_3 abundances in olivine it is likely that Bidi did not experience significant thermal metamorphism and therefore Bidi did not reside in a large body prior to incorporation into Wild 2 and was likely transported to the Kuiper belt directly from the solar nebula where chondrules formed.

ACKNOWLEDGMENTS

We wish to thank the Discovery and Cosmochemistry programs at NASA for support of the Stardust mission, funding of instrumentation and sample procurement. Special thanks to Hanson Fong of the Materials Science and Engineering Department, University of Washington, for FESEM assistance with obtaining backscatter images. We thank Trevor Ireland and two additional reviewers for constructive comments which improved the manuscript. This work was supported by NASA Grants NNX10AI89GS01 and NNX09AC30G. The WiscSIMS lab is partially funded by NSF-EAR (0319230, 0516725, 0744079, 1053466).

REFERENCES

Aléon J., Krot A. N. and McKeegan K. D. (2002) Calcium–aluminum inclusions and amoeboid olivine aggregates from the CR carbonaceous chondrites. *Meteorit. Planet. Sci.* **37**, 1729–1755.

Anderson W. W. (1998) Physics of interplanetary dust collection with aerogel. *NASA Technical Report*. NASA/CR-1998-207766. pp. 23.

Bayliss, P., Berry, L. G., Mrose, M. E. and Smith, D. D. (eds.) (1980) *JCPDS Mineral Powder Diffraction File Data Book*. JCPDS International Centre for Diffraction Data, Swarthmore, PA.

Bigolski J. N., Weisberg M. K., Connolly Jr. H. C. and Ebel D. S. (2013) Microchondrules in unequilibrated ordinary chondrites: insights into chondrule formation environments. *44th Lunar and Planetary Science Conference*. Lunar Planet. Inst., Houston, TX. # 2239 (abstr.).

Bischoff A. and Keil K. (1984) Al-rich objects in ordinary chondrites: related origin of carbonaceous and ordinary chondrites and their constituents. *Geochim. Cosmochim. Acta* **48**, 693–709.

Bockelée-Morvan D., Gautier D., Hersant F., Huré J.-M. and Robert F. (2002) Turbulent radial mixing in the solar nebula as the source of crystalline silicates in comets. *Astron. Astrophys.* **384**, 1107–1118.

Brearley A. J. and Jones R. H. (1998) Chondritic meteorites in planetary materials. In *Reviews in Mineralogy*, vol. 36 (ed. J. J. Papike). Mineralogical Society of America, Washington, DC.

Bridges J. C., Changela H. G., Nayakshin S., Starkey N. A. and Franchi I. A. (2012) Chondrule fragments from comet Wild 2: evidence for high temperature processing in the outer solar system. *Earth Planet. Sci. Lett.* **341–344**, 186–194.

Brigham C. A., Yabuki H., Ouyang Z., Murrell M. T., El Goresy A. and Burnett D. S. (1986) Silica-bearing chondrules and clasts in ordinary chondrites. *Geochim. Cosmochim. Acta* **50**, 1655–1666.

Brownlee D. E., Joswiak D. and Matrajt G. (2012) Overview of the rocky component of Wild 2 comet samples: insight into the early solar system, relationship with meteoritic materials and the differences between comets and asteroids. *Meteorit. Planet. Sci.* **47**, 453–470.

Burchell M. J., Fairey S. A. J., Wozniakiewicz P., Brownlee D. E., Hörz F., Kearsley A. T., See T. H., Tsou P., Westphal A., Green S. F., Trigo-Rodríguez J. M. and Domingúez G. (2008) Characteristics of cometary dust tracks in Stardust aerogel and laboratory calibrations. *Meteorit. Planet. Sci.* **43**, 23–40.

Ciesla F. J. (2007) Outward transport of high-temperature materials around the midplane of the solar nebula. *Science* **318**, 613–615.

Cliff G. and Lorimer G. W. (1975) The quantitative analysis of thin-sections. *J. Microsc.* **103**, 203–207.

Cuzzi J. N., Hogan R. C. and Shariff K. (2008) Toward planetesimals: dense chondrule clumps in the protoplanetary nebula. *Astrophys J* **687**, 1432–1447.

Dobrică E. and Brearley A. J. (2013) Ubiquitous microchondrules in the matrix of unequilibrated ordinary chondrites. *44th Lunar and Planetary Science Conference*. Lunar Planet. Inst., Houston, TX. #2701 (abstr.).

Fagan T. J., Krot A. N., Keil K. and Yurimoto H. O. (2004) Oxygen isotopic evolution of amoeboid olivine aggregates in the reduced CV3 chondrites Efremovka, Vigarano, and Leoville. *Geochim. Cosmochim. Acta* **68**, 2591–2611.

Franchi I. A. (2008) Oxygen isotopes in asteroidal materials. In *Oxygen in the Solar System, Reviews in Mineralogy and Geochemistry*, vol. 68 (ed. Glenn J. MacPherson). Mineralogical Society of America, pp. 345–397.

Gainsforth Z., Butterworth A. L., Bonal L., Brownlee D. E., Huss G. R., Joswiak D., Ogliore R. C., Telus M., Tyliczszak T. and Wesphal A. J. (2010) Chondrule fragments in Stardust tracks 113 and 154. 73rd Annual Meeting of the Meteoritical Society, held July 26–30 in New York, New York, Meteoritics and Planetary Science Supplement. #5428 (abstr.).

Ghiorso M. S. and Sack R. O. (1995) Chemical mass transfer in magmatic processes. IV. A revised and internally consistent thermodynamic model for the interpolation and extrapolation of liquid–solid equilibria in magmatic systems at elevated temperatures and pressures. *Contrib. Miner. Petrol.* **119**, 197–212.

Grossman J. N. and Brearley A. J. (2005) The onset of metamorphism in ordinary and carbonaceous chondrites. *Meteorit. Planet. Sci.* **40**, 87–122.

Guan Y., Huss G. R., Leshin L. A., MacPherson G. J. and McKeegan K. D. (2006) Oxygen isotope and ^{26}Al–^{26}Mg systematics of aluminum-rich chondrules from unequilibrated enstatite chondrites. *Meteorit. Planet. Sci.* **42**, 33–47.

Heck P. R., Ushikubo T., Schmitz B., Kita N. T., Spicuzza M. J. and Valley J. W. (2010) A single asteroidal source for extraterrestrial Ordovician chromite grains from Sweden and China: high-precision oxygen three-isotope SIMS analysis. *Geochim. Cosmochim. Acta* **74**, 497–509.

Hezel D. C., Palme H., Brenker F. E. and Nasdala L. (2003) Evidence for fractional condensation and reprocessing at high temperatures in CH chondrites. *Meteorit. Planet. Sci.* **38**, 1199–1215.

Hewins R. H. (1996) Chondrules and the protoplanetary disk: an overview. In *Chondrules and the Protoplanetary Disk* (eds. R. H. Hewins, R. H. E. Jones and E. R. D. Scott). Cambridge University Press, Cambridge, pp. 3–9.

Hiyagon H. and Hashimoto A. (1999) ^{16}O excesses in olivine inclusions in Yamato-86009 and Murchison chondrites and their relation to CAIs. *Science* **283**, 828–831.

Hörz F. et al. (2006) Impact features on stardust: implications for Comet 81P/Wild 2 dust. *Science* **314**, 1716–1719.

Imai H. and Yurimoto H. (2003) Oxygen isotopic distribution in an amoeboid olivine aggregate from the Allende CV chondrite: primary and secondary processes. *Geochim. Cosmochim. Acta* **67**, 765–772.

Ishi H., Stadermann F. J., Floss C., Joswiak D., Bradley J. P., Teslich N., Brownlee D. E., Matrajt G., MacPherson G. and McKeegan K. D. (2010) Lack of evidence for in situ decay of aluminum-26 in comet 81PWild 2 CAI-like refractory particles 'Inti' and 'Coki'. *41st Lunar and Planetary Science Conference*. Lunar Planet. Inst., Houston, TX. #2317 (abstr.).

Itoh S., Russell S. S. and Yurimoto H. (2007) Oxygen and magnesium isotopic compositions of amoeboid olivine aggregates from the Semarkona LL3.0 chondrite. *Meteorit. Planet. Sci.* **42**, 1241–1247.

Jones R. H. (1996) FeO-rich, porphyritic pyroxene chondrules in unequilibrated ordinary chondrites. *Geochim. Cosmochim. Acta* **60**, 3115–3118.

Jones R. H. and Scott E. R. D. (1989) Petrology and thermal history of type 1A chondrules in the Semarkona (LL3.0) chondrite. *Proceedings of the 19th Lunar and Planetary Science Conference*. pp. 523–536.

Jones R. H., Leshin L. A., Guan Y., Sharp Z. D., Durakiewicz T. and Schilk A. J. (2004) Oxygen isotope heterogeneity in chondrules from the Mokoia CV3 carbonaceous chondrite. *Geochim. Cosmochim. Acta* **68**, 3423–3438.

Jones R. H., Guan Y., Leshin L. A., Larsen T. and Sharp Z. D. (2005) Oxygen isotope distribution of NWA739, a CH chondrite with affinities to Acfer 182. *36th Lunar and Planetary Science Conference*. Lunar Planet. Inst., Houston, TX. #1813 (abstr.).

Joswiak D. J., Brownlee D. E., Matrajt G., Westphal A. J. and Snead C. J. (2009) Kosmochloric Ca-rich pyroxenes and FeO-rich olivines (Kool grains) and associated phases in Stardust tracks and chondritic porous interplanetary dust particles: possible precursors to FeO-rich type II chondrules in ordinary chondrites. *Meteorit. Planet. Sci.* **44**, 1561–1588.

Joswiak D. J., Brownlee D. E., Matrajt G., Messenger S. and Ito M. (2010) Stardust track 130 terminal particle: possible Al-rich chondrule fragment or altered amoeboid olivine aggregate. *41st Lunar and Planetary Science Conference*. Lunar Planet. Inst., Houston, TX. #2119 (abstr.).

Joswiak D. J., Brownlee D. E., Matrajt G., Westphal A. J., Snead C. J. and Gainsforth Z. (2012) Comprehensive examination of large mineral and rock fragments in Stardust tracks: mineralogy, analogous extraterrestrial materials and source regions. *Meteorit. Planet. Sci.* **47**, 471–524.

Joswiak D. J., Brownlee D. E. and Matrajt G. (2013) Newly discovered CAI in comet Wild 2: a refractory inclusion analogous to type C CAI precursors? 76th Annual Meeting of the Meteoritical Society, Edmonton, CA. #5136 (abstr.).

Keller Ch. and Gail H. P. (2004) Radial mixing in protoplanetary accretion disks. *Astron. Astrophys.* **415**, 1177–1185.

Kita N. T., Nagahara H., Togashi S. and Morishita Y. (2000) A short duration of chondrule formation in the solar nebula: evidence from ^{26}Al in Semarkona ferromagnesian chondrules. *Geochim. Cosmochim. Acta* **64**, 3913–3922.

Kita N. T., Ushikubo T., Fu B. and Valley J. W. (2009) High precision SIMS oxygen isotope analysis and the effect of sample topography. *Chem. Geol.* **264**, 43–57.

Kita N. T., Nagahara H., Tachibana S., Tomomura S., Spicuzza J. J., Fournelle J. H. and Valley J. W. (2010) High precision SIMS oxygen three isotope study of chondrules in LL3 chondrites: role of ambient gas during chondrule formation. *Geochim. Cosmochim. Acta* **74**, 6610–6635.

Kitamura M., Goto T. and Syono Y. (1977) Intergrowth textures of diaplectic glass and crystal in shock-loaded P-anorthite. *Contrib. Miner. Petrol.* **61**, 299–304.

Komatsu M., Krot A. N., Petaev M. I., Ulyanov A. A., Keil K. and Miyamoto M. (2001) Mineralogy and petrography of amoeboid olivine aggregates from the reduced CV3 chondrites Efremovka, Leoville and Vigarano: products of nebular condensation, accretion and annealing. *Meteorit. Planet. Sci.* **36**, 629–641.

Komatsu M., Mikouchi T. and Miyamoto M. (2009) High-temperature annealing of amoeboid olivine aggregates: heating experiments on olivine–anorthite mixtures. *Polar Sci.* **3**, 31–55.

Krot A. N. and Keil K. (2002) Anorthite-rich chondrules in CR and CH carbonaceous chondrites: genetic link between calcium–aluminum-rich inclusions and ferromagnesian chondrules. *Meteorit. Planet. Sci.* **37**, 91–111.

Krot A. N., Rubin A. E., Keil K. and Wasson J. T. (1997) Microchondrules in ordinary chondrites: implications for chondrule formation. *Geochim. Cosmochim. Acta* **61**, 463–473.

Krot A. N., Meibom A., Petaev M. I., Keil K., Zolenksy M. E., Saito A., Mukai M. and Ohsumi K. (2000) Ferrous silicate spherules with euhedral iron, nickel-metal grains from CH carbonaceous chondrites: evidence for supercooling and condensation under oxidizing conditions. *Meteorit. Planet. Sci.* **35**, 1249–1258.

Krot A. N., Hutcheon I. D. and Keil K. (2002a) Plagioclase-rich chondrules in the reduced CV chondrites: evidence for complex formation history and genetic links between calcium–aluminum-rich inclusions and ferromagnesian chondrules. *Meteorit. Planet. Sci.* **37**, 155–182.

Krot A. N., McKeegan K. D., Leshin L. A., MacPherson G. J. and Scott E. R. D. (2002b) Existence of an ^{16}O-rich gaseous reservoir in the solar nebula. *Science* **295**, 1051–1054.

Krot A. N., Fagan T. J., McKeegan K. D., Sahijpal S., Hutcheon I. D., Petaev M. I. and Yurimoto H. (2004a) Ca, Al-rich inclusions, amoeboid olivine aggregates, and Al-rich chondrules from the unique carbonaceous chondrite Acfer 094: I. Mineralogy and petrology. *Geochim. Cosmochim. Acta* **68**, 2167–2184.

Krot A. N., Petaev M. I., Russell S. S., Itoh S., Fagan T. J., Yurimoto H., Chizmadia L., Weisberg M. K., Komatsu M., Ulyanov A. A. and Keil K. K. (2004b) Amoeboid olivine aggregates and related objects in carbonaceous chondrites: records of nebular and asteroid processes. *Chem. Erde* **64**, 185–239.

Krot A. N., Yurimoto H., McKeegan K. D., Leshin L., Chaussidon M., Libourel G., Yoshitake M., Huss G. R., Guan Y. and Zanda B. (2006) Oxygen isotopic compositions of chondrules: implications for evolution of oxygen isotopic reservoirs in the inner solar nebula. *Chem. Erde* **66**, 249–276.

Kurahashi E., Kita N. T., Nagahara H. and Morishita Y. (2008) ^{26}Al–^{26}Mg systematics of chondrules in a primitive CO chondrite. *Geochim. Cosmochim. Acta* **72**, 3865–3882.

LaTourrette T. and Wasserburg G. J. (1998) Mg diffusion in anorthite: implications for the formation of early solar planetesimals. *Earth Planet. Sci. Lett.* **158**, 91–108.

Leitner J., Hoppe P. and Heck P. R. (2010) First discovery of presolar material of possible supernova origin in impact residues from comet 81P/Wild 2. *41st Lunar and Planetary Science Conference*. Lunar Planet. Inst., Houston, TX. #1609 (abstr.).

Leroux H., Jacob D., Stodolna J., Nakamura-Messenger K. and Zolensky M. (2008) Igneous Ca-rich pyroxene in comet 81P/Wild 2. *Am. Mineral.* **93**, 1933–1936.

Lofgren G. E. (1996) A dynamic crystallization model for chondrule melts. In *Chondrules and the Protoplanetary Disk* (eds. R. H. Hewins, R. H. Jones and E. R. D. Scott). Cambridge University Press, New York, pp. 187–196.

MacPherson G. J. and Huss G. R. (2005) Petrogenesis of Al-rich chondrules: evidence from bulk compositions and phase equilibria. *Geochim. Cosmochim. Acta* **69**, 3099–3127.

Makide K., Nagashima K., Krot A. N., Huss G. R., Hutcheon I. D. and Bischoff A. (2009) Oxygen- and magnesium-isotope compositions of calcium–aluminum-rich inclusions from CR2 carbonaceous chondrites. *Geochim. Cosmochim. Acta* **73**, 5018–5050.

Maruyama S. and Yurimoto H. (2003) Relationship among O, Mg isotopes and the petrography of two spinel-bearing compound chondrules. *Geochim. Cosmochim. Acta* **67**, 3943–3957.

Matrajt G. and Brownlee D. E. (2006) Acrylic embedding of Stardust particles encased in aerogel. *Meteorit. Planet. Sci.* **41**, 1695–1835.

Matrajt G., Ito M., Wirick S., Messenger S., Brownlee D. E., Joswiak D., Flynn G., Sandford S., Snead C. and Westphal A. (2008) Carbon investigation of two Stardust particles: a TEM, NanoSIMS and XANES study. *Meteorit. Planet. Sci.* **43**, 315–334.

Matzel J. E. P., Ishii H. A., Joswiak D., Hutcheon I. D., Bradley J. P., Brownlee D., Weber P. K., Teslich N., Matrajt G., McKeegan K. and MacPherson G. J. (2010) Constraints on the formation age of cometary material from the NASA Stardust mission. *Science* **328**, 483–486.

McKeegan K. D. et al. (2006) Isotopic compositions of cometary matter returned by Stardust. *Science* **314**, 1724–1728.

Messenger S., Joswiak D., Ito M., Matrajt G. and Brownlee D. E. (2009) Discovery of presolar SiC from comet Wild-2. *40th Lunar and Planetary Science Conference*. Lunar Planet. Inst., Houston, TX (DVD). #1790 (abstr.).

Misawa K. and Nakamura N. (1996) Origin of refractory precursor components of chondrules from carbonaceous chondrites. In *Chondrules and the Protoplanetary Disk* (eds. R. H. Hewins, R. H. Jones and E. R. D. Scott). Cambridge University Press, New York, pp. 99–105.

Miyamoto M., Koizumi E. and Mikouchi T. (2009) Cooling rates of Y980459 and DAG476 shergottites on the basis of Fe–Mg

zoning of olivine. *40th Lunar and Planetary Science Conference*. Lunar Planet. Inst., Houston, TX. #1143 (abstr.).

Nagahara H., Kita N. T., Ozawa K. and Morishita Y. (2008) Condensation of major elements during chondrule formation and its implication to the origin of chondrules. *Geochim. Cosmochim. Acta* **72**, 1442–1465.

Nakamura T., Noguchi T., Tsuchiyama A., Ushikubo T., Kita N. T., Valley J. W., Zolensky M. E., Kakazu Y., Sakamoto K., Mashio E., Uesugi K. and Nakano T. (2008) Chondrule-like objects in short-period comet 81P/Wild 2. *Science* **321**, 1664–1667.

Nakamura-Messenger K., Keller L. P., Clemett S. J., Messenger S. and Ito M. (2011) Nanometer-scale anatomy of entire Stardust tracks. *Meteorit. Planet. Sci.* **46**, 1033–1051.

Nakashima D., Ushikubo T., Rudraswami N. G., Kita N. T., Valley J. W. and Nagao K. (2011) Ion microprobe analyses of oxygen three-isotope ratios of chondrules from the Sayh al Uhaymir 290 CH chondrite using a multiple-hole disk. *Meteorit. Planet. Sci.* **46**, 857–874.

Nakashima D., Ushikubo T., Zolensky M. E. and Kita N. T. (2012) High precision oxygen three-isotope analyses of anhydrous chondritic interplanetary dust particles. *Meteorit. Planet. Sci.* **47**, 197–208.

Ogliore R. C., Huss G. R., Nagashima K., Butterworth A. L., Gainsforth Z., Stodolna J., Westphal A. J., Joswiak D. and Tyliszczak T. (2012) Incorporation of a late-forming chondrule into comet Wild 2. *Astrophys. J. Lett.* **745**, 1–5.

Palme H. and Jones A. (2004) Solar system abundances of the elements. In *Meteorites Comets and Planets* (ed. A. M. Davis). Elsevier B.V., Amsterdam, pp. 41–62.

Rubin A. E. (1989) An olivine-microchondrule-bearing clast in the Krymka meteorite. *Meteoritics* **24**, 191–192.

Rubin A. E. (2010) Physical properties of chondrules in different chondrite groups: implications for multiple melting events in dusty environments. *Geochim. Cosmochim. Acta* **74**, 4807–4828.

Rubin A. E., Scott E. R. D. and Keil K. (1982) Microchondrule-bearing clast in the Piancaldoli LL3 meteorite: a new kind of type 3 chondrite and its relevance to the history of chondrules. *Geochim. Cosmochim. Acta* **46**, 1763–1776.

Rudraswami N. G., Ushikubo T., Nakashima D. and Kita N. T. (2011) Oxygen isotope systematics of chondrules in the Allende CV3 chondrite: high precision ion microprobe studies. *Geochim. Cosmochim. Acta* **75**, 7596–7611.

Russell S. S., Srinivasan G., Huss G. R., Wasserburg G. J. and MacPherson G. J. (1996) Evidence for widespread ^{26}Al in the solar nebular and constraints for nebula time scales. *Science* **273**, 757–762.

Russell S. S., MacPherson G. J., Leshin L. A. and McKeegan K. D. (2000) ^{16}O enrichments in aluminum-rich chondrules from ordinary chondrites. *Earth Planet. Sci. Lett.* **184**, 57–74.

Sandford S. A. et al. (2006) Organics captured from comet 81P/Wild 2 by the Stardust spacecraft. *Science* **314**, 1720–1724.

Schmitz S., Brenker F. E., Schoonjans T., Vekemans B., Silversmit G., Vincze L., Burghammer M. and Riekel C. (2009) In situ identification of a CAI candidate in 81P/Wild 2 cometary dust by confocal high resolution synchrotron X-ray fluorescence. *Geochim. Cosmochim. Acta* **73**, 5483–5492.

Scott E. R. D. and Krot A. N. (2005a) Chondrites and their components. In *Meteorites, Comets and Planets*, vol. 1 (ed. A. M. Davis), pp. 143–200. Treatise on Geochemistry. Elsevier-Pergamon, Oxford.

Scott E. R. D. and Krot A. N. (2005b) Thermal processing of silicate dust in the solar nebula: clues from primitive chondrite matrices. *Astrophys. J.* **623**, 571–578.

Sheng Y. J. (1992) Origin of plagioclase-olivine inclusions. Ph. D. thesis, California Institute of Technology.

Shu F. H., Shang H., Glassgold A. E. and Lee T. (1997) X-rays and fluctuating X-winds from protostars. *Science* **277**, 1475–1479.

Simon S. B., Joswiak D. J., Ishii H. A., Bradley J. P., Chi M., Grossman L., Aléon J., Brownlee D. E., Fallon S., Hutcheon I. D., Matrajt G. and McKeegan K. D. (2008) A refractory inclusion returned by Stardust from comet 81P/Wild2. *Meteorit. Planet. Sci.* **43**, 1861–1877.

Stodolna J., Gainsforth Z., Butteroworth A. and Westphal A. J. (2012) TEM/STXM characterization of preserved primitive material from the comet Wild 2. *43rd Lunar and Planetary Science Conference*. Lunar Planet. Inst., Houston, TX. #1214 (abstr.).

Stolper E. and Paque J. M. (1986) Crystallization sequences of Ca–Al-rich inclusions from Allende: the effects of cooling rate and maximum temperature. *Geochim. Cosmochim. Acta* **50**, 1785–1806.

Tenner T. J., Nakashima D., Ushikubo T., Kita N. T. and Weisberg M. K. (2012) Oxygen isotopes of chondrules in the Queen Alexandria Range 99177 CR3 chondrite: further evidence for the systematic relationship between chondrule Mg# and Δ^{17}O and the role of ice during chondrule formation. *43rd Lunar and Planetary Science Conference*. Lunar Planet. Inst., Houston, TX. #2127 (abstr.).

Tenner T. J., Ushikubo T., Kurahashi E., Kita N. T. and Nagahara H. (2013) Oxygen isotope systematics of chondrule phenocrysts from the CO3.0 chondrite Yamato 81020: evidence for two distinct oxygen isotope reservoirs. *Geochim. Cosmochim. Acta* **102**, 226–245.

Tronche E. J., Hewins R. H. and MacPherson G. J. (2007) Formation conditions of aluminum-rich chondrules. *Geochim. Cosmochim. Acta* **71**, 3361–3381.

Ushikubo T., Kimura M., Kita N. T. and Valley J. W. (2012) Primordial oxygen isotope reservoirs of the solar nebula recorded in chondrules in Acfer 094 carbonaceous chondrite. *Geochim. Cosmochim. Acta* **90**, 242–264.

Valley J. W. and Kita N. T. (2009) In situ oxygen isotope geochemistry by ion microprobe. *Mineralogical Association of Canada Short Course*, vol. 41. pp. 19–63.

Wasson J. T. (1993) Constraints on chondrule origins. *Meteoritics* **28**, 14–28.

Wasson J. T. and Krot (1994) Fayalite-silica association in unequilibrated ordinary chondrites: evidence for aqueous alteration on a parent body. *Earth Planet. Sci. Lett.* **122**, 403–416.

Weinbruch S. and Müller W. F. (1995) Constraints on the cooling rates of chondrules from the microstructure of clinopyroxene and plagioclase. *Geochim. Cosmochim. Acta* **59**, 3221–3230.

Weisberg M. K. and Connolly H. C. (2008) On the relationship between chondrites, comets and asteroids, a petrologic perspective. *39th Lunar and Planetary Science Conference*. Lunar Planet. Inst., Houston, TX. #1981 (abstr.).

Weisberg M. K., Prinz M., Clayton R. N. and Mayeda T. K. (1993) The CR (Renazzo-type) carbonaceous chondrite group and its implications. *Geochim. Cosmochim. Acta* **57**, 1567–1586.

Weisberg M. K., Kita N. T., Ushikubo T., Connolly H. C. Jr., Ebel D. S., Spicuzza M. J., Valley J. W. (2007) Petrologic-isotopic study of amoeboid olivine aggregates in CR chondrites. *38th Lunar and Planetary Science Conference*. Lunar Planet. Inst., Houston, TX. #1588 (abstr.).

Weisberg M. K., Ebel D. S., Connolly, Jr., H. C., Kita N. T. and Ushikubo T. (2011) Petrology and oxygen isotope compositions of chondrules in E3 chondrites. *Geochim. Cosmochim.Acta* **75**, 6556–6569.

Weisberg M. K., Connolly H. C. and Ebel D. S. (2004) Petrology and origin of amoeboid olivine aggregates in CR chondrites. *Meteorit. Planet. Sci.* **39**, 1741–1753.

Westphal A. J., Snead C. J., Butterworth A. L., Graham G. A., Bradley J. P., Bajt S., Grant P. G., Bench G., Brennan S. and Pianetta P. (2004) Aerogel keystones: extraction of complete hypervelocity impact events from aerogel collectors. *Meteorit. Planet. Sci.* **39**, 1375–1386.

Wick M. J. and Jones R. H. (2012) Formation conditions of plagioclase-bearing type I chondrules in CO chondrites: a study of natural samples and experimental analogs. *Geochim. Cosmochim. Acta* **98**, 140–159.

Zolensky M. E. et al. (2006) Mineralogy and petrology of Comet 81P/Wild2 nucleus samples. *Science* **314**, 1735–1739.

Associate editor: Trevor Ireland